



Article

Real-Time Energy Optimal Control of Two-Stage Reverse Osmosis Desalination

Larry Gao, Yakubu A. Jarma, Panagiotis D. Christofides * and Yoram Cohen *

Chemical and Biomolecular Engineering Department, Water Technology Research Center, University of California, Los Angeles, CA 90095, USA

* Correspondence: pdc@seas.ucla.edu (P.D.C.); yoram@ucla.edu (Y.C.)

Abstract

A two-level model-based control system for energy-optimal operation of a two-stage reverse osmosis (RO) membrane desalination system was developed and field demonstrated. The control scheme was based on the specific energy consumption (SEC) framework accounting for pump efficiencies, physical system constraints, and temporal variability of feed salinity. The SEC framework consisted of a higher-level (supervisory) control system that guided a lower-level controller for real-time SEC optimization. The supervisory controller combined real-time plant data and the SEC model to determine the energyoptimal first-stage water recovery and the overall permeate water recovery (unless specified), and membrane permeability for a target permeate production. The derived operating state was then applied to control the RO plant operation through the lower-level control system, consisting of three separate feedback loops regulating the RO feed flow rate, first-stage RO pressure, and the second-stage RO pressure via control of the first-stage and second-stage RO feed pumps, and the RO concentrate valve. The two-level control system was demonstrated for a mobile brackish water desalination plant capable of permeate productivity up to 98 m³/day. Field testing demonstrated robust simultaneous control of the dynamically coupled control variables and effective energy-optimal operation.

Keywords: desalination; two-stage RO; energy-optimal operation; brackish water

Academic Editor: Jesus Gonzalez-Lopez

Received: 4 July 2025 Revised: 27 July 2025 Accepted: 4 August 2025 Published: 8 August 2025

Citation: Gao, L.; A. Jarma, Y.; Christofides, P.D.; Cohen, Y. Real-Time Energy Optimal Control of Two-Stage Reverse Osmosis Desalination. *Water* **2025**, *17*, 2363. https://doi.org/10.3390/w17162363

Copyright: © 2025 by the authors. Licensee MDPI, Basel, Switzerland. This article is an open access article distributed under the terms and conditions of the Creative Commons Attribution (CC BY) license (https://creativecommons.org/license s/by/4.0/).

1. Introduction

Reverse osmosis (RO) desalination is a leading technology for desalting inland brackish water and in water reuse applications [1–6], where increasing product water recovery is critical to reducing the volume of generated concentrate [7,8]. Product water (i.e., permeate) recovery can be increased by adding multiple RO stages [9–18], operating in the mode of partial concentrate recycle [19] or operating in batch or semi-batch mode [20–22]. Studies on multi-stage RO have largely focused on evaluating the potential for reducing energy consumption and increasing recovery through optimization of various system configurations with respect to the number and arrangement of membrane elements in the different RO stages, use of interstage booster pumps, and incorporation of energy recovery devices [3,13,23–27]. Here, it is noted that the traditional approach to increasing the recovery of brackish water desalination, and thus reducing the challenge of concentrate management, typically relies on a plant configuration that consists of two or three RO stages with interstage pumps [10,11,28].

Water 2025, 17, 2363 2 of 26

Irrespective of the particular multi-stage plant configuration, energy-optimal operation requires the determination of the optimal plant operational set-points. Here we note that previous studies on multi-stage RO systems have focused primarily on specific plant configurations (e.g., number of stages, number of elements per stage and their configuration, interstage pumps, and recycle flows). These studies have provided guidance regarding the dependence of the specific energy consumption (SEC) on operating conditions and some have addressed operational complexities that may be introduced due to system design constraints (e.g., lower and upper stage recovery limits, permeate flux constraint, minimum and maximum allowable pump outlet pressures, pump efficiencies), changing plant production targets and temporal variability of source water salinity [29–33].

The common industry practice in the operation of two-stage RO plants is to set the desalination plant operation so as to equalize the permeate flux between the two RO stages [11,25,34]. Such an approach, however, does not guarantee optimal SEC operation [35], as it does not consider the impact of the plant's physical and operational constraints on the attainable minimum SEC [36,37]. In theory, energy-optimal operation can be achieved provided that each one of the plant stages can operate up to its respective thermodynamic restriction limit, and all stage recoveries are equal [12]. Such an approach is practically unrealizable for actual RO plants given their physical and operational constraints. However, irrespective of the plant design and its physical equipment and operational constraints, reaching an energy-optimal operation of a multi-stage RO plant is desirable, and it can be achieved via optimization-based control [35]. Recently, simulations of energy-optimal control were presented for a two-stage low salinity RO system, whereby feed flow rate, first stage feed pressure, and interstage (i.e., second stage inlet) pressure controllers were guided by a data-driven model of system operation [38]. As noted in the above study, closed-loop (feedback) operational control (for dynamic SEC minimization), based on the use of data-driven system operation models, is constrained to the range of operating conditions for which the ML model was developed. Admittedly, plant operational ML models can be refined via reinforcement learning when sufficient new data are acquired. In contrast, however, mechanistic models of plant operation offer advantages such as (a) applicability over a wide range of conditions, (b) allowing for adaptation to external conditions (e.g., fouling progression, temperature) through real-time determination of membrane transport parameters (e.g., hydraulic permeability), (c) accounting for concentration polarization, and (d) mechanistic reasoning for operational trajectories toward the optimal operating conditions.

Considering the above and the need to establish energy-optimal control of two-stage RO operation, the present work introduces an optimization-based control scheme for a two-stage RO plant. The approach is based on the use of a supervisory controller that utilizes real-time plant sensor data, along with a plant SEC model, to determine the energy-optimal overall and per-stage recoveries for a given water productivity target. The established RO system operating states are then applied to control the plant operation through a lower-level controller, consisting of three separate feedback loops that regulate the RO plant feed flow rate, the first-stage RO pressure, and the second-stage RO pressure through the actuation of the first-stage RO feed pump, the second-stage RO feed pump, and the RO concentrate valve, respectively. The above-developed approach for real-time SEC minimization was implemented in a brackish water RO plant, and the control approach and system performance were field-demonstrated for multiple test cases that consider plant physical and operational constraints.

Water 2025, 17, 2363 3 of 26

2. Energy Optimization of Two-Stage RO

2.1. Two-Stage RO

Energy-optimal operational control of a two-stage RO system with an interstage booster pump was established for the system configuration shown in Figure 1, for which the relevant process variables are listed in Table 1. In this system, the booster pump raises the first-stage concentrate stream pressure to the target level for the feed to the second membrane stage. The overall water recovery, Y, for the two-stage RO system, and permeate recovery from the first (Y_1) and second (Y_2) RO stages are provided as follows:

$$Y = \frac{Q_p}{Q_{f,1}}, \quad Y_1 = \frac{Q_{p,1}}{Q_{f,1}}, \quad Y_2 = \frac{Q_{p,2}}{Q_{f,2}} = \frac{Q_p - Q_{p,1}}{Q_{f,1}(1 - Y_1)} = \frac{Y - Y_1}{1 - Y_1}$$
(1)

in which $Q_{f,1}$ and $Q_{f,2}$ are the first-stage (raw feed) and second-stage (concentrate from first stage) flow rates, while Q_p , $Q_{p,1}$, and $Q_{p,2}$ are the total, first-stage, and second-stage permeate flow rates, respectively. It is noted that for a prescribed overall permeate production flow rate (i.e., target Q_p), increasing the permeate production in the first stage will increase Y_1 and hence lower the required second-stage recovery (Y_2). Also, for a target overall recovery (Y_2), fixing Y_1 establishes the required second-stage recovery (i.e., Y_2).

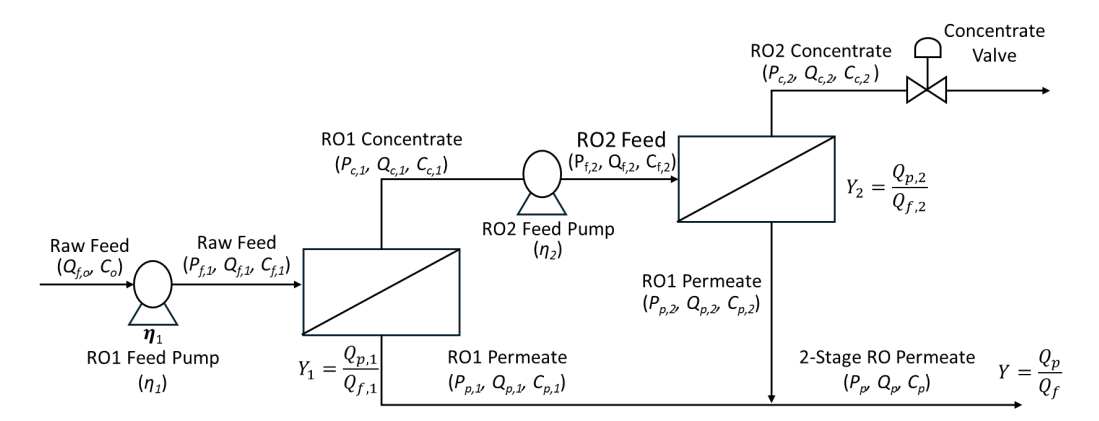


Figure 1. Schematic of a two-stage RO system. (P—pressure, Q—flow rate, C—salt concentration, Y—water recovery, η —pump efficiency, energy recovery device (ERD) can be added to the second stage, where subscripts f, c and p designate the feed, concentrate and permeate streams, respectively, and subscripts 1 and 2 identify the corresponding RO stages.

Table 1. Operating variables for the two-stage RO desalination plant.

	Flow Rate (Q)	Pressure (P)	Salinity (C)
Raw Feed	Q f	P_0	$C_{f,1} = C_o$
RO First-Stage Feed	$Q_{f,1} = Q_{f,o} = Q_f$	$P_{f,1}$	$C_{f,1} = C_o$
RO First-Stage Concentrate	$Q_{f,2}(Q_{c,1})$	$P_{c,1}$	Cc,1
RO Second-Stage Feed	$Q_{c,1} = Q_{f,2}$	$P_{f,2}$	$C_{f,2} = C_{c,1}$
RO Second-Stage Concentrate	$Q_{c,2}$	$P_{c,2}$	$C_{c,2}$
RO First-Stage Permeate	$Q_{p,1}$	$P_{p,1}$	<i>C</i> _{<i>p</i>,1}
RO Second-Stage Permeate	$Q_{p,2}$	$P_{p,2}$	$C_{p,2}$

2.2. SEC for a Two-Stage RO

The total energy consumption for the two-stage RO process (W_{Total}), shown in Figure 1, is the sum of the work performed by the first-stage pump (W_1) and the second-stage pump (W_2), minus the energy recovered (W_{ERD}) from the second-stage concentrate.

Water 2025, 17, 2363 4 of 26

$$W_{Total} = W_1 + W_2 - W_{ERD} \tag{2}$$

$$W_1 = \frac{\Delta P_1 \cdot Q_f}{\eta_1}$$
 and $W_2 = \frac{\Delta P_2 \cdot Q_f (1 - Y_1)}{\eta_2}$ (3)

$$W_{ERD} = (\Delta P_1 + \Delta P_2) \cdot (1 - Y) \cdot Q_f \cdot \eta_{ERD}$$
(4)

in which η_1 and η_2 are the first-stage and second-stage (interstage) pump efficiencies, respectively, η_{ERD} is the energy recovery device (ERD) efficiency, ΔP_1 is the first stage applied feed pressure relative to the raw source water feed pressure, i.e., $\Delta P_1 = P_{f,1} - P_0$), where P_0 is the raw feedwater pressure, and ΔP_2 is the pressure applied by the second-stage pump (relative to the first-stage exit concentrate pressure, i.e., $\Delta P_2 = P_{f,2} - P_{c,1}$. The total work performed per produced permeate volume, expressed as the specific energy consumption for the two-stage RO ($SEC_{(2RO)}$), is provided as follows:

$$SEC_{(2RO)} = \frac{W_{Total}}{Q_n} = \frac{\Delta P_1}{Y \cdot \eta_1} + \frac{\Delta P_2 \cdot (1 - Y_1)}{Y \cdot \eta_2} - \frac{(\Delta P_1 + \Delta P_2) \cdot (1 - Y) \cdot \eta_{ERD}}{Y}$$
 (5)

in which the first and second terms on the right-hand side of Equation (5) represent the first-stage and second-stage SEC values, respectively, and the third term accounts for the recovered energy if recovered via an installed ERD.

It is noted that, for each given stage, when the applied RO feed pressure (relative to the ambient pressure, i.e., ΔP_1) is equal to the transmembrane osmotic pressure difference at the RO membrane exit regions for each RO stage), the RO system operation reaches the thermodynamic crossflow restriction, and the SEC is at its global minimum. Under the above condition, the RO system operation is up to the thermodynamic restriction whereby the osmotic pressures of the concentrate streams at the exits from the first ($\pi_{1,exit}$) and second ($\pi_{2,exit}$) stages are given as:

$$\pi_{1,exit} = \Delta P_1 = \frac{\pi_0 R_1}{(1 - Y_1)}, \quad \pi_{2,exit} = \Delta P_1 + \Delta P_2 = \frac{\pi_0 R_T}{(1 - Y_1)}$$
(6a)

where R_1 and R_T are the first stage and overall salt rejection, respectively, given by:

$$R_1 = 1 - \frac{C_{p,1}}{C_f}, \quad R_T = 1 - \frac{C_p}{C_f}$$
 (6b)

in which the salinity of the Stage 1 and Stage 2 feed, and overall permeate are denoted by C_f , $C_{p,1}$, and C_p , respectively.

RO desalination plants are not expected to operate up to the limit imposed by the thermodynamic restriction [12,13,39]. Nonetheless, it is of interest to assess the impact of efficiencies of the first- and second-stage pumps on the SEC, for a target overall recovery (*Y*), for operation up to such a limit. Accordingly, utilizing Equations (5) and (6a,b), and the reasonable approximation of negligible frictional losses and their impact on the SEC-optimal operating conditions, the SEC at the thermodynamic restriction, normalized with respect to the raw feed osmotic pressure, is given as follows:

$$SEC_{tr,norm}(2ROs) = \frac{SEC}{\pi_0} = \frac{R_1}{\eta_1 Y (1 - Y_1)} + \frac{1}{\eta_2 Y} \left[\frac{R_T (1 - Y_1)}{(1 - Y)} - R_1 \right] - \frac{R_T \cdot \eta_{ERD}}{Y}$$
(7)

in which, as in Equation (5), the first and second terms on the right-hand side of Equation (7) are the contributions of the first and second RO stages to the SEC, respectively, and the third term is the recovered energy if an ERD is utilized in the system. When, for a given

Water 2025, 17, 2363 5 of 26

plant where both stages operate up to the thermodynamic restriction limit, the desired water productivity dictates the overall product water recovery. The optimal Stage 1 recovery $(Y_{1,optimal})$ for a given overall recovery (Y) is thus obtained by setting $\partial[SEC_{tr,norm}(2ROs)]/\partial Y_1 = 0$ and solving to obtain [12].

$$Y_{1,optimal} = 1 - \sqrt{\frac{R_1 \cdot \eta_2}{R_T \cdot \eta_1} (1 - Y)}$$
(8)

As shown in Figures 2 and 3, for a fixed overall recovery, when the Stage 2 feed pump efficiency is above that of the Stage 1 pump (i.e., $\eta_2/\eta_1 > 1$), $Y_{1,optimal}$ for minimizing the SEC, increases as the first-stage pump efficiency increases. Conversely, when the Stage 1 pump efficiency is higher relative to the Stage 2 pump, for a given overall recovery, it can be shown (based on Equations (7) and (8)) that SEC minimization would be reached at a lower optimal Stage 1 recovery (Y_1 , optimal).

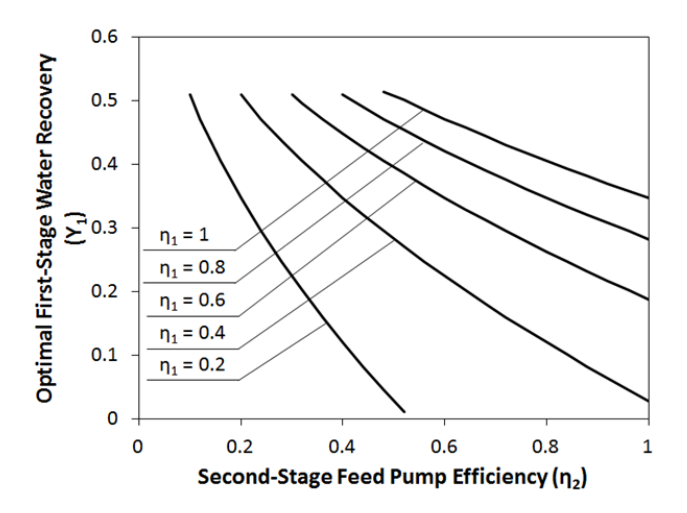


Figure 2. Profiles of the optimal operating Stage 1 water recovery (Y_1) as a function of the Stage 1 and Stage 2 pump efficiencies (i.e., η_1 and η_2 , respectively) as per Equation (8).

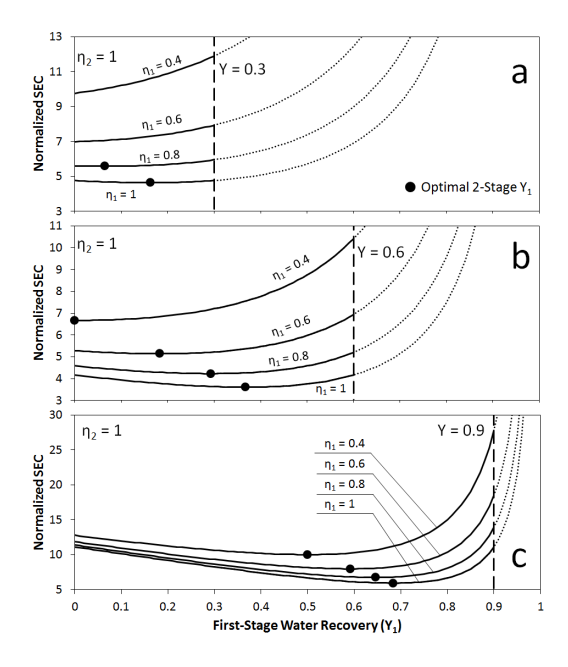


Figure 3. Plot of SEC vs. first-stage water recovery (Y_1) at a fixed overall water recovery (Y) of (a) 30%, (b) 60%, and (c) 90%, constant η_2 = 1 and varying η_1 . As η_2 decreases, SEC increases, and the optimal Y_1 increases. SEC curves were calculated through Equation (7).

Water 2025, 17, 2363 6 of 26

2.3. RO System Operation at a Constrained Permeate Flow Rate and the Applied First and Second Stage Inlet Pressures

The operational objective for an RO plant is typically to provide a constant permeate productivity (i.e., flow rate), and this constraint must be considered when optimizing the RO system operation with respect to the SEC. For a two-stage RO plant, the permeate flow rate from the first and second stages, $Q_{p,i}$ (i = 1, 2 denotes the first and second stages, respectively), can be expressed as per the classical RO permeate flux equation [40]:

$$Q_{p,i} = A_{m,i} L_{p,i} \left(\overline{\Delta P_{m,i}} - \overline{\Delta \pi_i} \right) \tag{9}$$

where $A_{m,i}$ is the active membrane surface area, $L_{p,i}$ is the membrane permeability coefficient, and $\overline{\Delta P_{m,i}}$ is the applied (average) transmembrane pressure. The average osmotic pressure difference across the membrane is defined as $\overline{\Delta \pi_i} = (\overline{\pi_i} - \overline{\pi_{p,i}})$, in which $\overline{\pi_i}$ and $\overline{\pi_{p,i}}$ are the average osmotic pressures at the membrane surface and permeate streams, respectively, for RO stage i. The average transmembrane osmotic pressure can be reasonably approximated by the log-mean average along each of the plant stages [41,42]

$$\overline{\Delta \pi_i} = \pi_{0,i} \frac{ln\left(\frac{1}{1 - Y_i}\right)}{Y_i} \overline{(CP)_i} - \pi_{0,i} \left(1 - R_i\right)$$
(10)

in which $\pi_{0,i}$ is the stage i feedwater osmotic pressure, $\overline{(CP)_i}$ is the average concentration polarization modulus along the membrane train (i.e., $\overline{(CP)_i} = C_{m,i}/C_{b,i}$, where C_b and C_m are the average salt concentrations in the bulk and at the membrane surface, respectively, and R_i is the RO stage i salt rejection (i.e., $R_i - 1 - C_p/\overline{C}_m$). Considering the axial pressure profile linearity along the RO element train, the average transmembrane pressure can be expressed as $\overline{\Delta P_{m,i}} = \left(P_{f,i} + P_{c,i}\right)/2 - P_{p,i}$, in which $P_{f,i}$, $P_{c,i}$, and $P_{p,i}$ are the feed, exit concentrate, and permeate pressures, respectively. Following the above, the stage i permeate flow rate and corresponding feed pressure are given as [35]:

$$Q_{p,i} = A_{m,i} L_{p,i} \left[\frac{P_{f,i} + P_{c,i}}{2} - P_{p,i} - \frac{\pi_{0,i}}{Y_i} ln \left(\frac{1}{1 - Y_i} \right) \cdot \left(\overline{CP} \right)_i + \pi_{0,i} \cdot \frac{C_{p,i}}{C_{f,i}} \right]$$
(11)

$$P_{f,i} = 2 \left[\frac{Q_{p,i}}{A_{m,i} L_{p,i}} + P_{p,i} + \frac{\pi_{0,i}}{Y_i} ln \left(\frac{1}{1 - Y_i} \right) \cdot \left(\overline{CP} \right)_i + \pi_{0,i} \cdot \frac{C_{p,i}}{C_{f,i}} - P_{c,i} \right]$$
(12)

in which $A_{m,i}$ and $L_{p,i}$ are the stage i membrane active surface area and permeability coefficients, respectively, $C_{p,i}$ is the stage i permeate concentration. The individual stage permeate flow rates can then be expressed in terms of the overall target permeate flow rate (Q_p) and the overall recovery (Y), and the individual stage recoveries (Y_i) . Accordingly, the Stage 1 and Stage 2 permeate flow rates are given as $Q_{p,1} = Q_p (Y_1/Y)$ and $Q_{p,2} = Q_p (1 - Y_1/Y)$, respectively. Thus, the required inlet (feed) pressures for the first $(P_{f,1})$ and second $(P_{f,2})$ stage can be expressed as:

$$P_{f,1} = 2 \left[Q_{p,norm}^{1} \left(\frac{Y_{1}}{Y} \right) + P_{p,1} + \frac{\pi_{0,1}}{Y_{1}} \ln \left(\frac{1}{1 - Y_{1}} \right) \cdot \left(\overline{CP} \right) + \pi_{0,1} \cdot \frac{C_{p,1}}{C_{f,1}} \right] - P_{c,1}$$
 (13a)

Water 2025, 17, 2363 7 of 26

$$P_{f,2} = 2 \left[Q_{p,norm}^2 \left(\frac{Y - Y_1}{Y} \right) + P_{p,2} + \frac{\pi_{0,2}}{\left(Y - Y_1 \right)} \ln \left(\frac{1 - Y_1}{1 - Y} \right) \cdot \left(\overline{CP} \right)_2 + \pi_{0,2} \cdot \frac{C_{p,2}}{C_{f,2}} \right] - P_{c,2}$$
 (13b)

in which
$$Q_{p,norm}^{(1)}=Q_p/\left(A_{m,1}L_{p,1}\right)$$
 and $Q_{p,norm}^{(1)}=Q_p/\left(A_{m,1}L_{p,1}\right)$, and where the concentration

tion polarization modulus for each stage can typically be determined utilizing the manufacturer-reported relations for the specific RO elements used in the plant [35,43].

2.4. Energy-Optimal Control of Two-Stage RO

2.4.1. Overall Control Scheme and Supervisory RO Controller

A two-level control scheme was developed to enable driving the RO system to its energy-optimal operation, with respect to the overall system recovery, considering the constraint imposed by the target permeate productivity. The control architecture, which was previously demonstrated for a single-stage RO system [35], consists of supervisory-level and lower-level controllers. The supervisory controller determines the energy-optimal operational set-points toward which the lower-level controller drives the system.

The supervisory controller utilizes real-time process sensor data and then computes, using the most recent sensor data, the Stage 1 and Stage 2 membrane permeabilities (via rearrangement of Equation (13a,b). The membrane permeability is computed prior to each required sequence of control actions, and thus the actual membrane performance is considered (at the prevailing temperature and membrane fouling condition). Once the membrane permeabilities are computed (with the latest sensor data), Equations (13a,b) are used to calculate the first- and second-stage feed inlet pressures required to attain the target total permeate flow rate for the total recovery (*Y*) and first-stage recovery (*Y*₁). Subsequently, the SEC for the two-stage RO system is determined using Equation (5) based on the pressure set-points. Next, the overall recovery and Stage 1 recovery (*Y* and *Y*₁, respectively) are calculated. The *Y*₁ and *Y* operational set-points that minimize the SEC can then be determined by numerically solving the constrained optimization problem as specified in Table 2, where the inequality constraints are the permissible plant operating ranges.

It is emphasized that the constraints on the recoveries (*Y*, *Y*₁) are due to functional limitations on the pressure, permeate flux, and crossflow velocity for the installed RO elements, and the number of elements per stage. Additional constraints on the feed flow rates and output pressure are imposed by the operational ranges for the first- and second-stage feed pumps, and upper limit pressure constraints imposed on the RO pressure vessels. In addition, the efficiencies of the pumps, which vary with flow rate and pressure output [44], impact the energy-optimal operating states of the RO system. Moreover, the efficiencies of the pumps, which vary with flow rate and pressure output [44], impact the energy-optimal operating states of the RO system [36,45]. Therefore, in the present control scheme, the variability of pump efficiencies was considered, as detailed in Appendix A.1.

The constrained nonlinear SEC optimization problem for the RO plant, as described by the equations and constraints listed in Table 2, was solved using the sequential quadratic programming method [46]. In this approach, once the optimal overall recovery ($Y_{optimal}$) and Stage 1 recovery ($Y_{1,optimal}$) are first determined (Figure 4), the permeate flow rates and feed pressures are then calculated via Equations (11), (12), and (13a,b), respectively; these values are the set-points provided to the lower-level controller (Figures 4 and 5). The lower-level controller drives the RO system to its new operational state, while the supervisory controller remains idle until the system converges to the new set-points. In the present control scheme, the process of set-point calculations and application was considered as a single iteration by the supervisory controller. At the start of the subsequent iteration, the updated plant sensor values (e.g., pressures, flow rates, conductivities) and

Water 2025, 17, 2363 8 of 26

the membrane permeabilities were used for the next round of supervisory control calculations. Evaluation of the controller's performance (i.e., with respect to maintaining permeate productivity and energy-optimal operation) was carried out subject to step changes in the permeate production set-point and also considering short-term tests with temporally variable RO feedwater salinity (Section 3.3). Here we note that, based on preliminary step change tests with the RO plant (Section 2.4.2), an iteration time of at most 300 s was sufficient for the lower-level controller to drive the system to the required set-points. It is stressed that the above controller response time is significantly shorter than the typical long continuous operating time (days to months) for the RO system and the slow seasonal temporal variability of water quality and groundwater temperature.

Table 2. RO System operational equations and constraints (a).

$\min_{Y, Y_1} \left(SEC_{2Stage} \right) = \frac{\Delta P_1}{Y \cdot \eta_1} + \frac{\Delta P_2 \cdot (1 - Y_1)}{Y \cdot \eta_2}$		
a. $Q_p = Q_{p,set\text{-point}}$	h. $\eta_2 = h_2(\Delta P_2, Q_{f,2})$, Equation (A1b)	
$b. \Delta P_1 = P_{f,1} - P_O$	$i. Y_{min} \le Y \le Y_{max}$	
c. $\Delta P_2 = P_{f,2} - P_{c,1}$, Equation (13a)	$j. (Y_1)_{min} \le Y_1 \le (Y_1)_{max}; k. Y_1 < Y$	
d. $P_{f,2} = g_2(Q_p, Y, Y_1)$, Equation (13b)	l. $(Q_{f,1})_{min} \le Q_{f,1} \le (Q_{f,1})_{max}$	
$e. Q_{f,1} = Q_p / Y$	$m. (Q_{f,2})_{min} \le Q_{f,2} \le (Q_{f,2})_{max}$	
$f. Q_{f,2} = Q_f \left(1 - Y_1 \right)$	$n. (P_{f,1})_{min} \le P_{f,1} \le (P_{f,1})_{max}$	
g. $\eta_1 = h_1(\Delta P_1, Q_{f,1})$, Equation (A1a)	0. $(P_{f,2})_{min} \le P_{f,2} \le (P_{f,2})_{max}$	

⁽a) The pump efficiencies are provided in Appendix A.1.

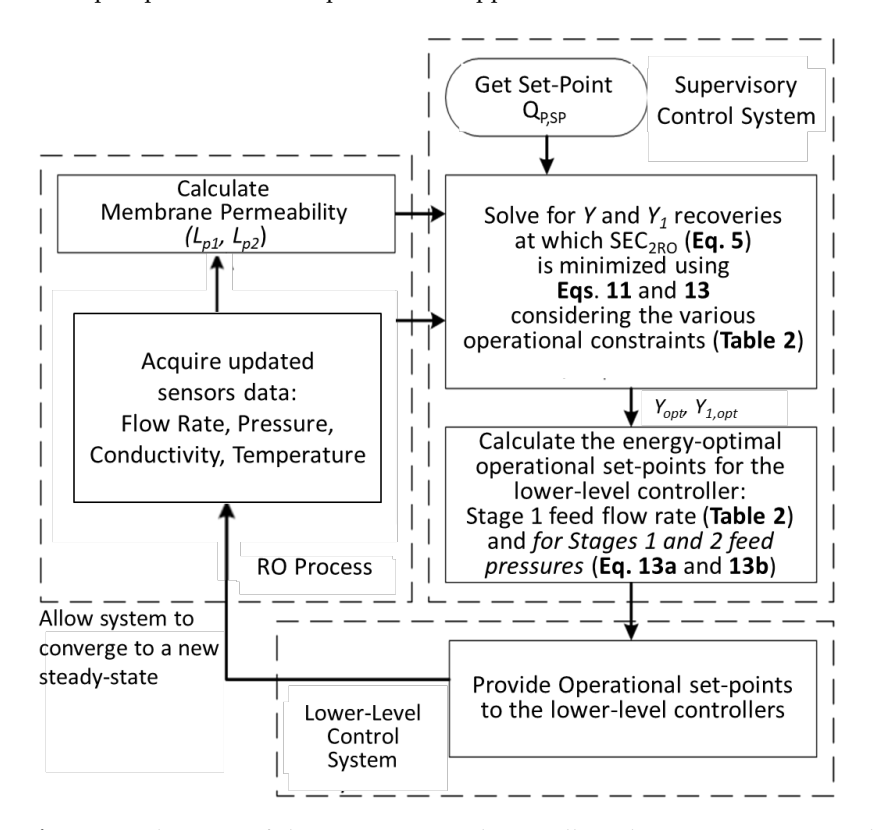


Figure 4. Schematic of the energy-optimal controller. The supervisory controller determines the overall recovery (Y) and Stage 1 recovery (Y_1) at which the system operation is at its energy-optimal state, and the lower-level controller drives the RO system toward these set-points.

Water 2025, 17, 2363 9 of 26

2.4.2. Lower-Level RO Controller

In the implementation of the overall control scheme, the lower-level controller (Figures 4 and 5) receives the feed flow rate (Q_f), the first-stage feed pressure ($P_{f,1}$), and the second-stage feed pressure ($P_{f,2}$) as set-points from the supervisory controller (based on the established optimal Y and Y_1 values; Section 2.4.1). Unlike energy-optimal control of a single-stage RO system [35], which requires two control variables (i.e., feed flow rate and feed pressure), the two-stage RO configuration requires simultaneous control of three dynamically coupled variables (e.g., the first-stage raw water feed flow rate, and the Stage 1 and Stage 2 inlet feed pressures).

In principle, a multivariable controller design can be used to account for multi-loop interactions [47–49] (Figure 4, Section 2.4.1). Here, it is noted that, unlike the energy-optimal control of a single-stage RO system [35], which requires only two control variables (i.e., feed flow rate and feed pressure), the two-stage RO configuration requires simultaneous control of three dynamically coupled variables (e.g., the first-stage raw water feed flow rate, and the first- and second-stage inlet feed pressures). In principle, a multivariable controller design can be used to account for multi-loop interactions [47,50]. However, such an approach would be at the expense of increasing computational demand and decreasing the level of modularity of the overall control architecture. Hence, given the above considerations, a simple control architecture with three control single-loops [51] was adopted with provisions implemented to enable fast response while avoiding overshoots when using multiple control loops. The approach was implemented by pairing a process output variable with the manipulated input variables and ordering the pairing in the order of decreasing strength of coupling [51]. To facilitate the above, preliminary step change tests were carried out with the two-stage RO plant (Section 3.1) to identify control pairings in the following order of relevance: (i) first-stage feed pump VFD control to regulate the RO Stage 1 feed flow rate, (ii) second-stage feed pump VFD control to regulate the first-stage inlet feed pressure, and (iii) second-stage concentrate valve control to regulate the secondstage feed pressure (Figure 5).

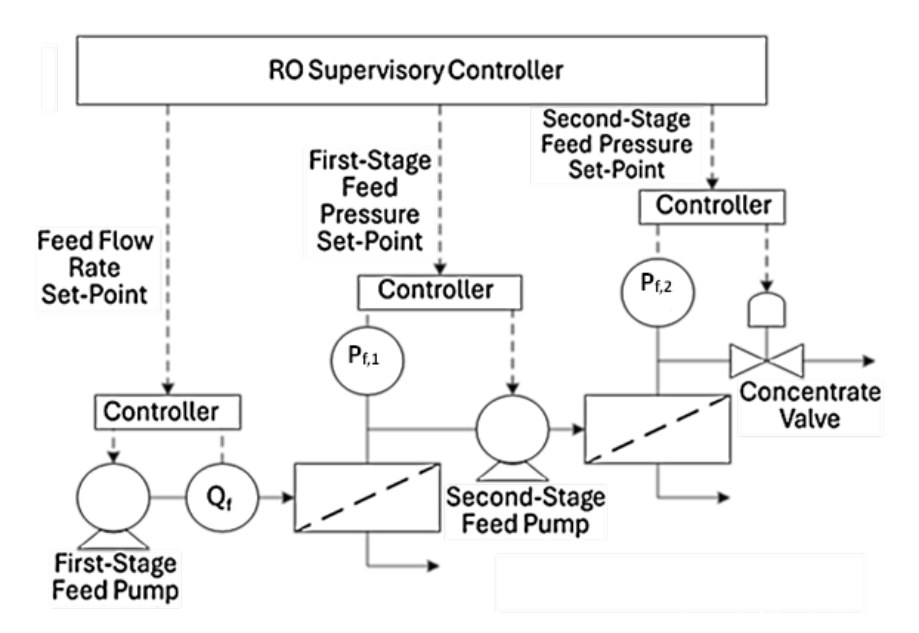


Figure 5. Illustration of the control architecture and the three feedback control loops for the two-stage RO system. The intermediate booster pump (i.e., second-stage pump) acts as a "concentrate valve" for the first stage, which provides controls over the first-stage feed pressure.

For the two-stage RO control system with three single control loops (Figure 5), the most sensitive control loop was tuned first. This is followed by the less sensitive control

Water 2025, 17, 2363 10 of 26

loops in sequence, and then reducing the gain and/or increasing the integral time for the controller of the least sensitive loop to ensure stability and avoid oscillations [51]. In the present two-stage RO control system with three single control loops (Figure 5), the most sensitive control loop is tuned first. This is followed by the less sensitive control loops in sequence, and then reducing the gain and/or increasing the integral time for the controllers of the least sensitive loops so as to ensure stability and avoid oscillations [51]. For the present RO system (Figure 1) and the control architecture (Figures 4-6), the control loop regulating the feed flow rate through the first-stage feed pump was determined to be the primary of the three control loops. This is not surprising since the first-stage feed pump drives fluid flow through the entire system; hence, it impacts the recovery as well as the pressure profile along the RO element train. The secondary control loop regulates the firststage feed pressure via control of the second-stage feed pump VFD, and thus it also impacts the feed pressures of the second RO stage. The third control loop is for adjustment of the second-stage concentrate valve for further tuning of the second-stage inlet pressure. The supervisory controller and the three lower-level control loops are shown schematically in Figure 6.

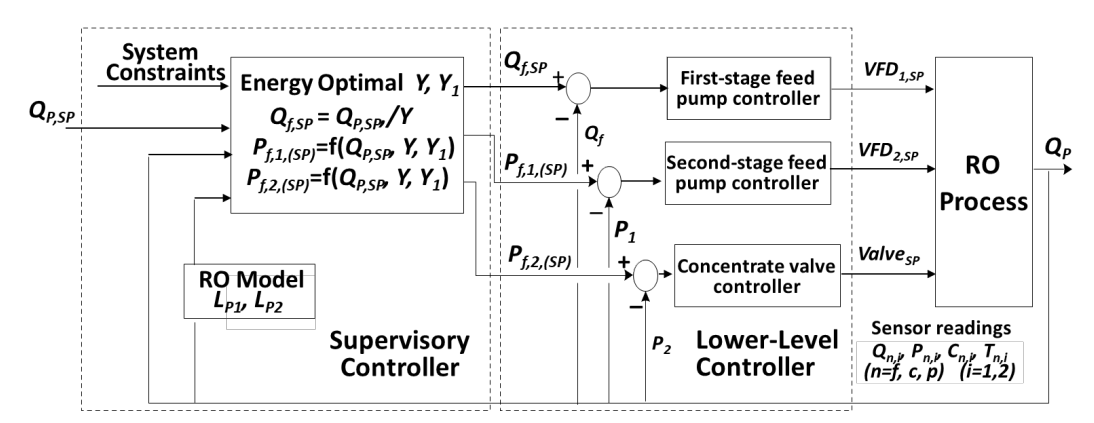


Figure 6. Process control diagram for the RO system consisting of a supervisory controller and three lower-level control loops. The supervisory controller establishes the flow rate and pressure setpoints for the lower-level controller. The first, second, and third control loops are for the first-stage feed pump (regulating the raw feed flow rate), the second-stage feed pump (regulating the first-stage inlet feed pressure), and the concentrate valve (tuning the second-stage feed pressure), respectively.

3. Experimental

3.1. Two-Stage RO Desalination System

The control scheme for energy-optimal operation of a two-stage RO system (Section 2.4) was evaluated based on field test with a containerized brackish RO pilot plant (Figures 1 and 7) having permeate production capacity of up to ~98 m³/day at 75% recovery (single pass) and up to 111 m³/day at 85% recovery with partial concentrate recycle. The plant was equipped with an array of sensors (conductivity, pH, temperature, and turbidity), flow meters, and pressure transducers interfaced with a data acquisition system and an onboard computer with a programmable control system. The RO desalination system was deployed at the Panoche Drainage District, CA (~428 km north of Los Angeles) for desalting agricultural drainage water of seasonally varying salinity (~11,000–19,000 mg/L total dissolved solids (TDS)) and turbidity (0.1–1.2 NTU).

Raw feedwater was fed from a groundwater sump pump and passed through a centrifugal separator (Lakos, Lindsay Corporation, Fresno, CA, USA) to a 0.57 m³ feedwater tank. Aluminum chlorohydrate (ACH) coagulant was then added to the feed (0.8 mg/L

Water 2025, 17, 2363 11 of 26

ACH) to increase the filtration efficiency prior to delivery to the RO unit. The chemically treated feed was then passed through a screen filter (2" Brushaway Filter, Amiad, Mooresville, NC, USA) for removal of particles > 300 μm. Subsequently, the feed stream was filtered via an ultrafiltration (UF) unit, consisting of two multi-channel hollow-fiber (insideout) UF elements (0.02 μm nominal pore size and 60 m² active membrane area per element; Dizzer XL 0.9 MB 60 W, Inge, Greifenberg, Germany). The UF-treated feed, which was directed to a 1.7 m³ UF filtrate tank, provided treated RO feedwater of turbidity < 0.1 NTU, which was sufficiently below the recommended maximum limit of <1 NTU for RO desalting [1,41]. The UF filtered water, which was pumped from the pretreated feedwater tank (1.7 m³) via a first-stage booster pump (CRN5-4 A-P-G-E-HQQE 1.5 HP, Grundfos, Bjerringbro, Denmark), was dosed with 5 mg/L of Flocon 135 antiscalant to suppress mineral scaling. This stream was directed to the first stage via high-pressure RO feed pump inlet (CRNE3-23 HS-P-GI-E-HQQE 10 HP, Grundfos, Bjerringbro, Denmark. The RO plant was operated with a high-pressure inter-stage booster pump (i.e., Stage 2 feed pump; CRNE 1-23 HS HS-P-GI-E-HQQE 6.2 HP, Grundfos, Bjerringbro, Denmark) that raised the Stage 1 concentrate pressure to the prescribed Stage 2 RO inlet pressure. Each of the highpressure pumps was operated via a separate independent variable frequency drive (VFD). The produced permeate was directed to a 1.7 m³ product water tank.

The first RO stage of the RO plant (Figure 7) consisted of fourteen brackish water RO membrane elements (4-inch TM710D RO elements, Toray, Poway, CA, USA), and the second RO stage consisted of seven RO membrane elements (4-inch TM810V RO elements, Toray, Poway, CA, USA). The first-stage and second-stage membrane elements were reported by the manufacturer to provide permeate flow rates of 9.8 m³/day for 2000 mg/L TDS feedwater (at 15% recovery, and 15.5 bar applied pressure) and 7.2 m³/day for 32,000 mg/L TDS feedwater (at 8% recovery, and 55.2 bar applied pressure), respectively. For both membrane types, salt rejection was reported to be 99.8%. The concentration polarization moduli for the RO element train in the first and second plant RO stages were determined based on the manufacturer's relations for the above specific elements (Appendix A.2) in the two stages.



Figure 7. (Left) Mobile two-stage RO plant trailer, and (right) inside view of the plant.

3.2. Lower-Level RO Controller Tuning

The lower-level controller served to drive the RO system toward the set-points, received from the Supervisory Controller, for Stage 1 feed flow rate and feed pressures for Stages 1 and 2 (Section 2.4.2, Figure 5). The above was accomplished via autonomous control adjustments of the first stage VFDs, the second stage RO pumps, and the percentage opening of the second stage concentrate valve (Figures 5 and 6), as per the following proportional integral (PI) controllers:

Water 2025, 17, 2363 12 of 26

$$VFD_{1,SP} = K_{p,1} \left(Q_{f,SP} - Q_f(t) \right) + \frac{K_{p,1}}{\tau_{1,1}} \int_0^t \left(Q_{f,SP} - Q_f(\tau) \right) d\tau$$
 (14a)

$$VFD_{2,SP} = K_{p,2} \left(P_{f,1,(SP)} - P_{f,1}(t) \right) + \frac{K_{p,2}}{\tau_{2,2}} \int_{0}^{t} \left(P_{f,1,(SP)} - P_{f,1}(\tau) \right) d\tau$$
 (14b)

$$Valve_{SP} = K_{p,3} \left(P_{f,2,(SP)} - P_{f,2}(t) \right) + \frac{K_{p,3}}{\tau_{2,3}} \int_{0}^{t} \left(P_{f,2,(SP)} - P_{f,2}(\tau) \right) d\tau$$
 (14c)

where $VFD_{i,SP}$ is the VFD set-point (0–100%) for the first- (i = 1) and second-stage (i = 2) feed pumps, $K_{P,j}$ are the proportional constants corresponding to the three PI controllers (j = 1,2 and 3), $Valves_P$ is the Stage 2 concentrate valve opening set-point (0–100%), and $\tau_{i,j}$ are the integral time constants for controller j (= 1–3) corresponding to Stages 1 and 2 (i = 1 and 2, respectively). Q_f , and Q_f , s_P are the Stage 1 measured and set-point feed flow rates, respectively, and $P_{f,1}$, $P_{f,2}$, and $P_{f,1,(SP)}$, $P_{f,2,(SP)}$ are the measured first- and second-stage feed pressure, and first- and second-stage set-point feed pressure, respectively. Tuning the individual control loops was based on initial system tests, whereby the PI parameters (Table 3) were established for decoupling the three control loops (Figure 6) and minimizing oscillations.

Table 3. Proportional and integral (PI) control constants for the lower-level PI controllers.

Proportional Constant	Integral Constants $(au_{i,j})$
$K_{p,1} = 0.529 \cdot VFD_1 \text{ (\%/LPM)}$	40 s
$K_{p,2} = -36.259 \cdot VFD_2 \text{ (%/MPa)}$	100 s
$K_{p,3} = -0.435 \ Valve \ (\%/MPa)$	100 s

3.3. RO System Control Tests

Four different control tests were conducted to assess the lower-level controller response. In the first test, plant operation was established for a specific raw RO Stage 1 feed flow rate, and first- and second-stage feed pressures (Section 4.2). Each of the above operating parameter values was then raised by ~20% as new set-points to evaluate the PI control loops. The second control test served to demonstrate energy-optimal control for a scenario of a target overall recovery (Y), whereby controller activation followed an initial RO operation that proceeded as per the conventional approach of permeate flux equality between the two RO stages [41]. In this second test, the SEC was optimized with respect to the permeate load distribution between the two RO stages for a given RO feed flow rate and operation at a fixed overall recovery (Section 4.3). The third control test focused on reducing the overall RO system SEC through simultaneous optimization of both the overall (Y) and Stage 1 (Y_1) recoveries. In this test, the RO system was initially operated at a target permeate flow rate with the RO plant set to operate at the same permeate flux for each of the two RO stages. Once a stable system operation was attained, the control system was activated. The supervisory controller then determined the operational set-points needed by the lower-level controller to guide the system operation toward the optimal Y and Y_1 to achieve the minimum SEC (Section 4.4). Finally, the fourth test focused on assessing the control strategy for SEC minimization upon increased feedwater salinity (Section A.4.). In this test, the RO system was first operated at a high element inflow salinity of 24,290 mg/L TDS, which was achieved via RO system operation with partial concentrate recycled to the first stage inlet. Concentrate recycling was then gradually decreased and eventually turned off, which transitioned the feedwater salinity to that of the raw feedwater salinity of 17,833 mg/L TDS.

Water 2025, 17, 2363 13 of 26

4. Results and Discussion

4.1. Overview

Field tests for the development and evaluation of the two-stage RO energy-optimal control strategy included the following steps (Section 3.3): (a) demonstration of the lower-level controller tuning (Section 4.2), (b) optimization of the first RO stage recovery (Y_1) under the imposed condition of a constant overall recovery (Y) (Section 4.3), (c) optimization of both Y_1 and Y (Section 4.4), and (d) evaluation of the performance of the control scheme under conditions of changing feedwater salinity Section A.4.).

4.2. Lower-Level RO Controller Performance

In the first control test, the lower-level controller's response to set-point changes for the three control loops was evaluated based on an initial plant operational status of raw water feed flow rate of 75.7 L/min, first-stage feed pressure of 1.84 MPa, and a second-stage pressure of 2.66 MPa. The set-points for each PI controller were subsequently changed to 90.8 L/min, 2.17 MPa, and 3.16 MPa, respectively (Figures 8a-8c). As shown in Figure 8, the three controllers converged to the new set-points without major oscillations. The feed flow rate set-point (Figure 8a) was reached within ~150 s, and the pressure set-points for Stages 1 and 2 were reached within ~280 s (Figure 8b) and ~430 s (Figure 8c), respectively. It is noted that minor overshooting of Stages 1 and 2 feed pressures is evident in Figure 8b (~ 0.11 MPa) and Figure 8c (~0.15 MPa), respectively. These pressure overshoots are not due to controller tuning but are attributed to the fastest control loop (Figure 8a), which regulates the Stage 1 feed flow rate, which, in turn, also impacts the control of the Stages 1 and 2 feed pressures.

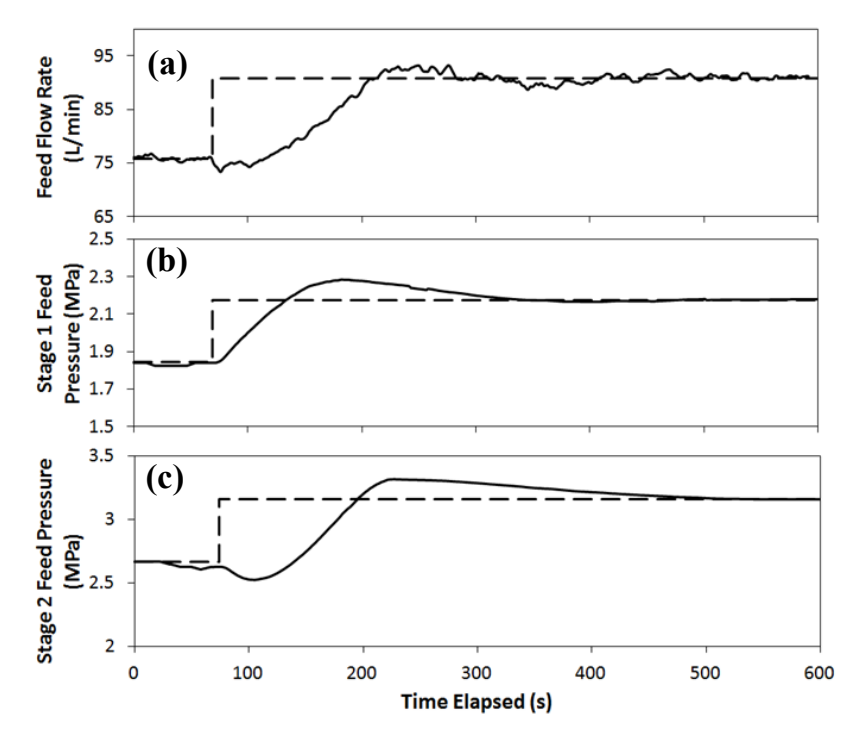


Figure 8. Time evolution of (**a**) RO feed flow rate, (**b**) RO Stage 1 feed pressure, and (**c**) RO Stage 2 feed pressure, whereby the set-points for the three controllers were changed simultaneously at 70s from (**a**) 75.7 L/min to 90.8 L/min, (**b**) 1.84 MPa to 2.17 MPa, and (**c**) 2.66 MPa to 3.16 MPa. Note: the Stage 1 feed flow rate and pressure, and Stage 2 feed pressure, were primarily impacted by the control of the Stages 1 and 2 pumps, and the concentrate valve, respectively.

In the implemented control scheme, when the Stage 1 feed flow rate controller (Figure 8a) detects a positive error (i.e., measured flow rate that is lower than its set-point), it

Water 2025, 17, 2363 14 of 26

responds by increasing the first-stage pump's RPM, which then raises the inlet pressures of both the first and second RO stages (Figure 8b and Figure 8c, respectively). Therefore, although inlet pressure controllers for the first and second RO stages are tuned at a slower timescale, slight overshoots can occur, as shown in Figure 8b,c. It is stressed that variability of water quality typically occurs over time-scales of days to months [31–33]; hence, the much shorter convergence time by lower-level controllers did not hinder plant operation.

4.3. SEC Reduction via Optimization of First-Stage Recovery for a Given Overall Recovery

In the second test, plant operation was first established for an overall recovery (i.e., Y = 74%) with an overall permeate water productivity set-point of 60.6 L/min, and Stage 1 feedwater salinity of ~11,591 mg/L TDS. Plant operation was set for the condition of permeate flux equalization between the two RO stages such that each stage operated with a permeate flux of 22.6 L/m²h, and whereby the Stage 1 recovery (Y_1) was 52% (Figure 9). For the above scenario, the first stage feed flow rate set-point was 81.8 L/min, and the feed pressures were 1.88 MPa and 2.77 MPa for the first and second RO stages, respectively. Once stable RO system operation was achieved, the energy-optimal control scheme was activated. The energy-optimal Stage 1 recovery (Y_1) was then determined by the supervisory controller, along with the corresponding pressures and flow rate set-points, as per the solution of the constrained nonlinear optimization problem (Section 2.4).

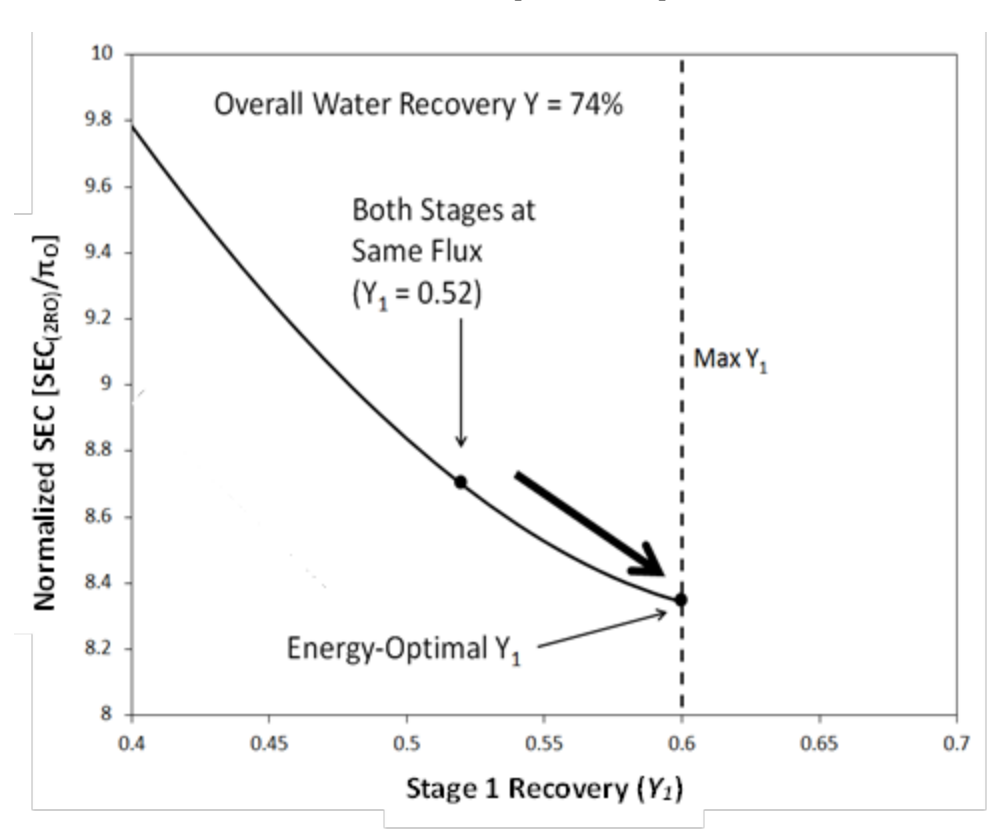


Figure 9. Normalized SEC dependence on Stage 1 recovery (Y_1) subject to constraints of overall recovery (Y = 74%) and max Stage 1 recovery ($Y_{1,max} = 60\%$) for a target permeate flow rate set-point of $Q_p = 60.6$ L/min. Solid circles denote the controller established operating points (Section 2.4).

The minimum SEC was determined for operation at the optimal Stage 1 recovery $(Y_{1,optimal})$ of 60%, which was the maximum achievable Stage 1 recovery $(Y_{1,max})$ for Stage 1 given the number and type of installed membrane elements (Section 3.1). As shown in Figure 9, the SEC decreased as the first-stage recovery (i.e., Y_1) increased, as predicted based on the constrained optimization problem (Section 2.4). It is noted that for the current

Water 2025, 17, 2363 15 of 26

RO system, the efficiency of the first-stage pump was higher than that of the second stage during the initial operating conditions (i.e., η_1 = 0.47 and η_2 = 0.34 at Y_1 = 52%). Also, the first-stage pump's efficiency increased further relative to the interstage (second-stage) pump (i.e., η_1 = 0.48 and η_2 = 0.3) as Y_1 increased to 60%. As Y_1 increased, along with the rise in the first-stage feed pressure, the Stage 1 pump efficiency (η_1 , Equation A1a) increased, while both the flow rate and pressure output of the second-stage pump decreased, accompanied by decreased second-stage pump efficiency (η_2). Considering the above, as Y_1 increased, η_2 decreased, and as a consequence, the optimal Y_1 increased toward the maximum possible Y_1 (i.e., the constraint of $Y_{1,max}$). The SEC at the optimal Y_1 (Figure 9) was reduced by ~4.2%, for the target overall recovery and permeate production, relative to the initial operating condition of flux equality between the two RO stages. The establishment of the feed pressure set-points to Stages 1 and 2, and subsequent control actions toward the optimal operating conditions are shown in Figures 9–11.

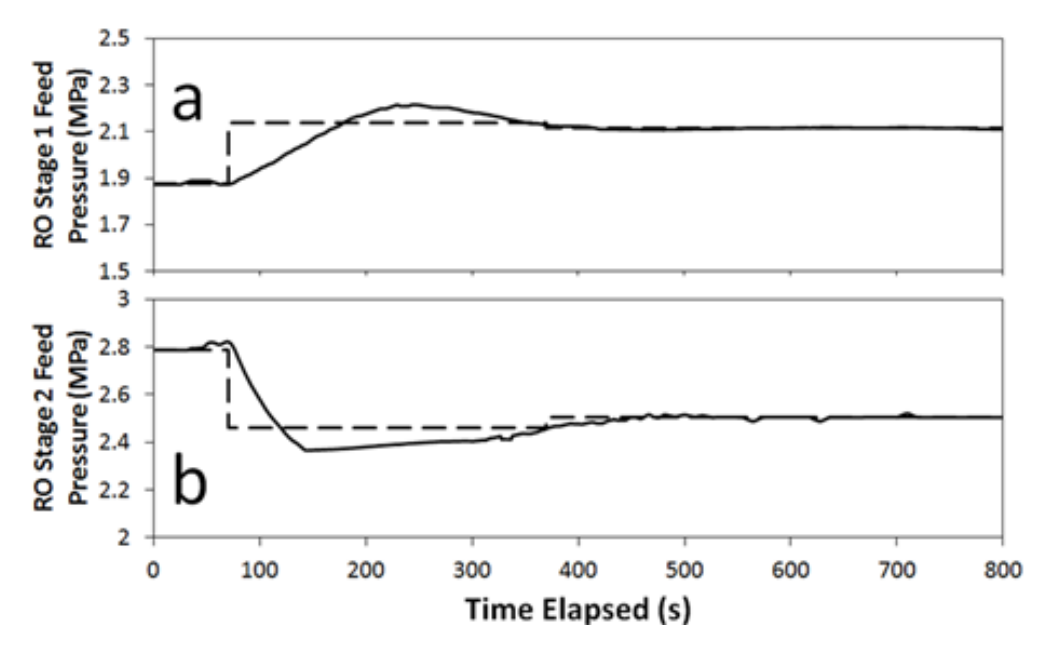


Figure 10. Profiles of (a) RO first-stage feed pressure and (b) RO Stage 2 feed pressure with respect to time. The RO Stage 1 feed pressure set-point was changed from 1.88 MPa to 2.11 MPa, while the RO Stage 2 feed pressure set-point changed from 2.79 MPa to 2.50 MPa.

During the transition from the initial first-stage recovery of Y_1 = 52% to 60%, the flow rates and pressures required to achieve the optimal Y_1 of 60% were determined by the supervisory controller and provided as set-points to the lower-level controllers. In the first iteration, the supervisory controller calculated a first-stage and second-stage inlet feed pressures of 2.14 MPa and 2.46 MPa, respectively. After ~300 s, the supervisory controller recalculated the required pressures and provided to the lower-level controllers the feed pressure set-points of 2.11 MPa and 2.50 MPa for the first and second stages, respectively. The transitions with respect to flow rates and pressures are illustrated in Figures 10 and 11, respectively. The control system drove the Stage 1 recovery (Y_1) upward by increasing its feed pressure (Figure 10a) while maintaining the permeate productivity set-point (Figure 11a,b) and the overall water recovery (by maintaining the feed flow rate, Figure 9).

Water 2025, 17, 2363 16 of 26

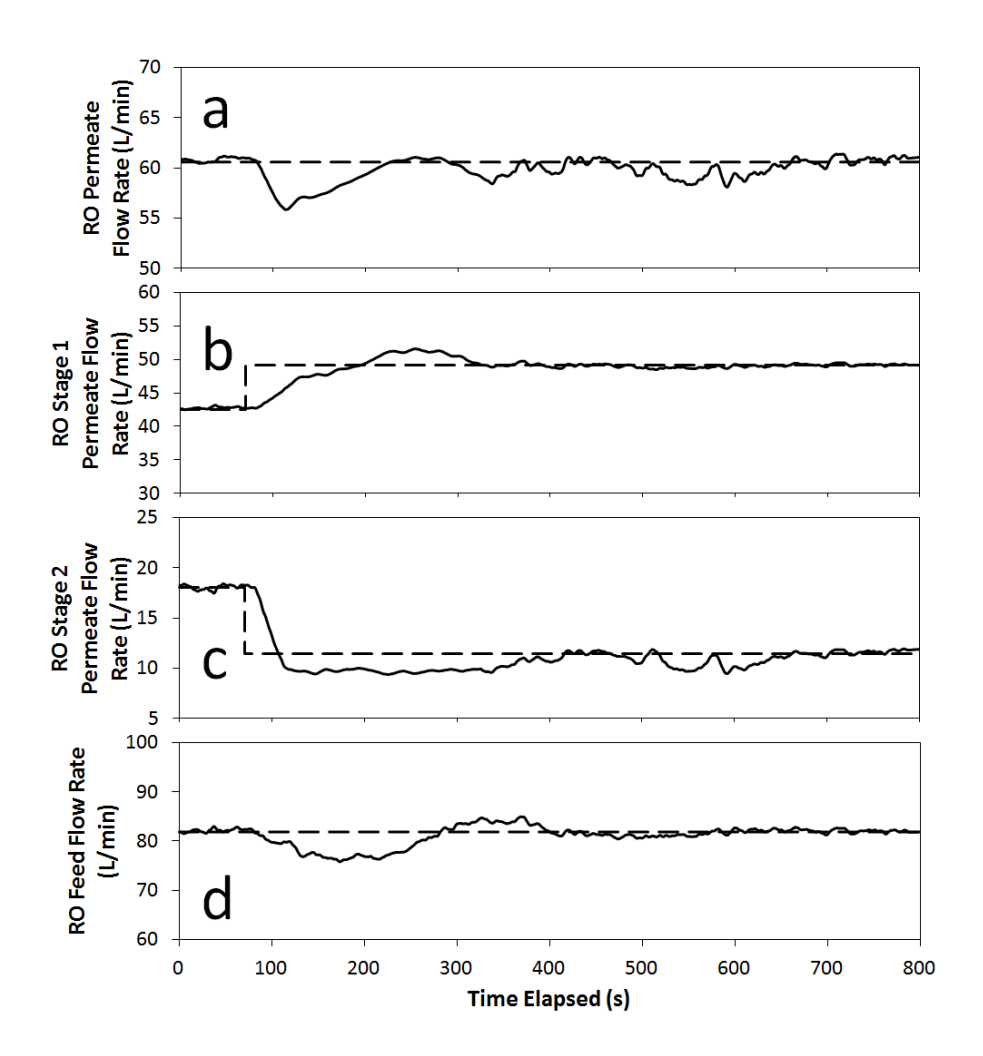


Figure 11. Time evolution of Two-Stage RO plant total (**a**) and Stages 1 (**b**) and 2 (**c**) permeate flow rates, respectively, and raw water feed flow rate (**d**). (Stage 1 recovery set-point was increased from $Y_1 = 0.52$ to 0.6. Constant overall permeate flow-rate, Stage 1 feed flow rate, and overall water recovery set-points were $Q_p = 60.6$ L/min, $Q_{p1} = 81.8$ L/min, and Y = 0.74, respectively.

4.4. SEC Reduction via Optimization of Both Stage 1 Recovery (Y1) and Overall Recovery (Y) for a Target Permeate Productivity

SEC minimization through simultaneous optimization of both the overall and Stage 1 recoveries (Y and Y_1 , respectively) was demonstrated in the third test (Section 3.3). In this test (Section 3.3), the RO system was initially set to desalt raw feedwater of salinity of 17,326 mg/L TDS with both Stages 1 and 2 operating at the same permeate flux of 17.0 L/m²h, corresponding to the overall and Stage 1 recoveries of Y = 74%, $Y_1 = 52\%$, respectively (Figure 12), permeate production of 45.4 L/min, and raw water feed flow rate of 61.4 L/min. For the above operation, Stages 1 and 2 feed pressures were 2.07 MPa and 3.50 MPa, respectively (Figure 13a,b). The controller was then activated and determined the Y and Y_1 values, which would result in a minimum SEC (Section 2.4), while the Stage 1 and 2 permeate flow rates were established via the system controller (Figure 14). Here we note that the Stage 1 permeate recovery was constrained for the current plant configuration and by the manufacturer-specified element upper pressure limit (i.e., max $P_{f,1}$ = 2.41 MPa). However, in this third test, the maximum allowable first stage pressure was set to 2.17 MPa (about 10% below the manufacturer's specified upper pressure constraint) to ensure equipment safety. Considering the various operational limitations, the attainable overall RO system recovery (Y) was in the constrained range of 40%–74%, with the operational region (with respect to the overall recovery and attained SEC shown in Figure 12.

Water 2025, 17, 2363 17 of 26

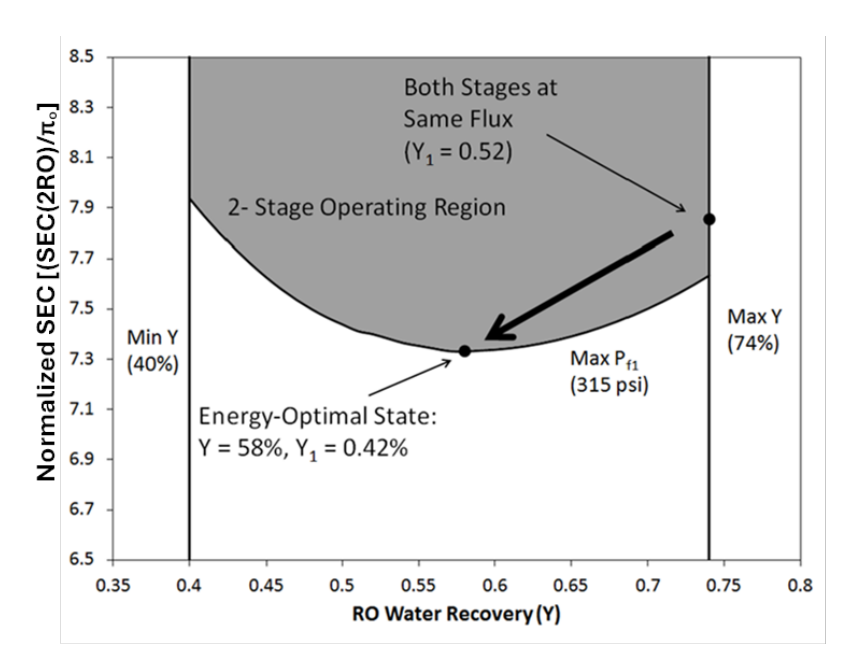


Figure 12. Normalized SEC (i.e., $SEC_{(2RO)}/\pi_{0}$) variation with the overall 2-stage recovery (Y) for operation subject to the constraints of minimum Y (40%), maximum Y (74%), and maximum $P_{f,1}$ (2.17 MPa). (Note: Solid dots denote the controller's established operating points, and the thick arrow indicates the transition from initial to energy-optimal state. (Note: the bounded SEC versus Y operational area was determined, as described in Appendix A.3.

Once a stable system operation was reached, the controller was activated, and the supervisory controller established the recovery set-points of Y_1 = 42% and Y = 58% (Figure 12) to attain the minimum SEC (for the target overall permeate production of 45.4 L/min), as described in Section 2.4. Accordingly, the Stage 1 raw water feed flow rate was autonomously adjusted (by the system controller) from the initial value to 61.4 L/min to 78.3 L/min, while the Stages 1 and 2 inlet pressures were adjusted from 2.07 MPa to 2.17 MPa, and from 3.50 MPa to 2.82 MPa, respectively. The transition to the optimal SEC operating conditions (Figures 13 and 14) occurred within a period of ~300 s, which is significantly shorter relative to the time scales of temporal variability (days to months) of the target permeate productivity demand and raw feedwater salinity.

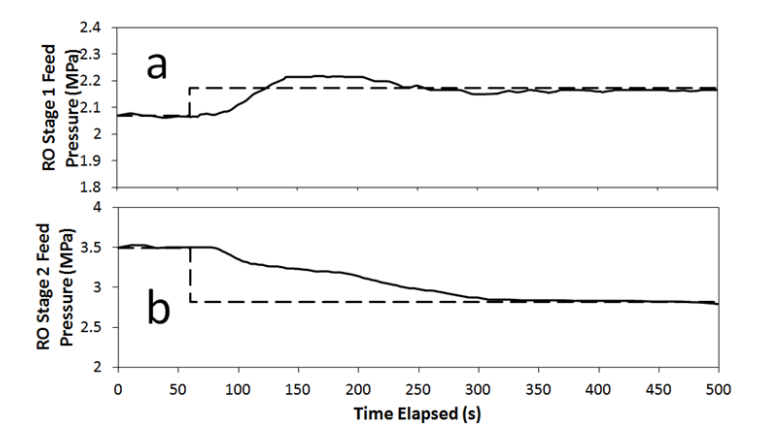


Figure 13. Profiles of (a) RO first-stage feed pressure and (b) RO second-stage feed pressure with respect to time. The feed pressure controller set-points were changed from (a) 2.07 MPa to 2.17 MPa and (b) 3.50 MPa to 2.82 MPa.

Water 2025, 17, 2363 18 of 26

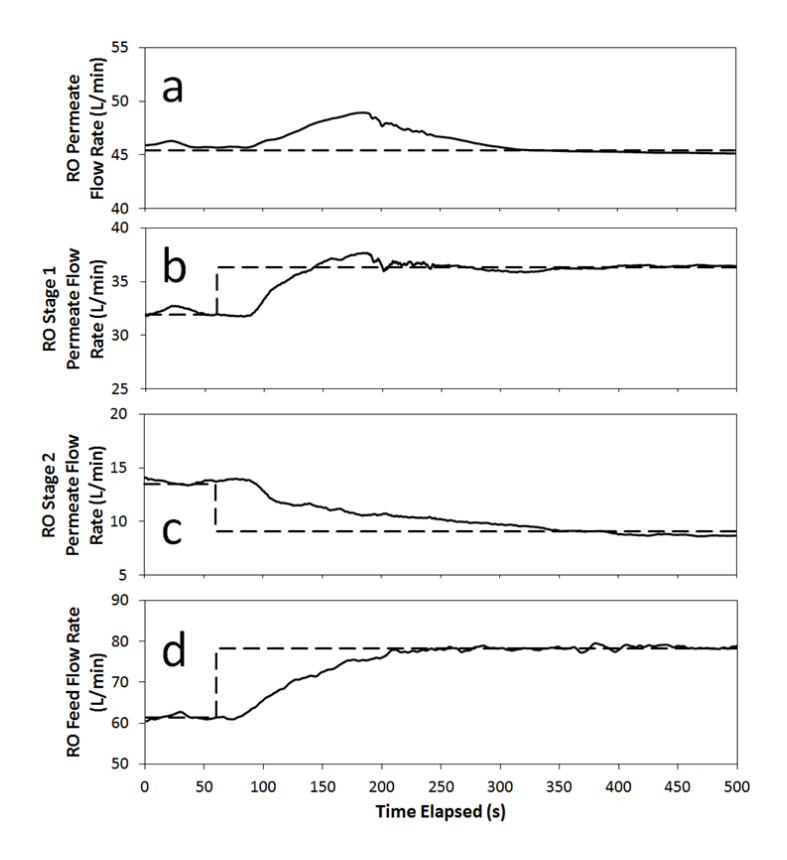


Figure 14. Profiles of (a) RO permeate flow rate, (b) RO first-stage permeate flow rate, (c) RO second-stage permeate flow rate, and (d) RO feed flow rate with respect to time. The controller established set-point changes were from Y = 74% to Y = 58%, $Y_1 = 0.52$ to $Y_1 = 0.42$, and feed flow rate change from 61.4 L/min to 78.3 L/min.

The changes in Y, Y_1 , the corresponding SEC transition to the optimal operating condition, at the constraint of maximum first-stage pressure, are shown in Figure 12. At the optimal operational state for a fixed permeate productivity, the SEC was ~7.1% lower relative to conventional operation of flux equality between the two RO stages. However, this necessitates operating at a lower overall recovery and higher raw source water feed flow rate (Figure 14d), which leads to a greater volume of RO concentrate. Here we note that SEC minimization for two-stage RO desalination, where both the overall recovery and overall permeate flow rate are fixed (Section 4.3), is preferred since a lower SEC is achieved, relative to operation with flux equalization and SEC optimization with respect to both Y_1 and Y for a given permeate productivity, without the penalty of increased generation of concentrate volume. The latter optimization scenario is also illustrated for the case where the raw water feed salinity changes during the operation (Appendix A.4).

4.5. Operational Control During Scenario of Changing Feed Salinity

The fourth test, which is described in Appendix A.4, was conducted to assess the control system's performance in response to a disturbance of increased water salinity. In this test, SEC optimal plant operation was established for a feed salinity of 24,190 mg/L TDS for a permeate production of 45.4 L/min, resulting in an overall recovery of 69% and Stage 1 recovery of 27.3%. The feed salinity was then gradually decreased to 17,833 mg/L TDS, and the system controller established the new operation to an overall recovery of 58% and Stage 1 recovery of 41.5%. The SEC was found to be about 10% lower than achieved with the conventional approach of flux equalization between the two stages. However, this was at the expense of operating at a lower overall recovery and thus a greater volume of generated RO concentrate. Therefore, it is clear that the operational

Water 2025, 17, 2363 19 of 26

decision must also consider energy savings versus the potential cost increase for the higher level of concentrate management.

5. Conclusions

A novel model predictive control (MPC) approach for energy-optimal operation of a two-stage RO membrane desalination system was developed and field-demonstrated for a brackish water desalination plant with a permeate production capacity of up to 98 m³/day. Specific energy consumption (SEC) was used as a framework to develop the model for minimizing the SEC for a two-stage RO system. The SEC model and SEC optimization approach, and control algorithms, along with real-time plant sensors data, served to solve for the SEC-optimal values for the overall (Y) and first-stage permeate recovery (Y1) for a given target water productivity, feed salinity, and membrane permeability. The operating state, which was determined by the supervisory controller, was then applied to a brackish water RO plant through its lower-level control system. The lowerlevel controller consisted of three separate feedback loops controlling the RO feed flow rate, the first-stage RO pressure, and the second-stage RO pressure through actuation of the first-stage RO feed pump, the second-stage RO feed pump, and the RO concentrate valve, respectively. The control system was successfully field-demonstrated for desalting brackish groundwater through effective energy-optimal operation enabled by simultaneous control of dynamically coupled operational variables. Additional reduction in operational costs also involves various additional operational strategies, including, but not limited to, production scheduling to take advantage of periods of low electricity rates with considerations of product water storage constraints, in addition to optimal scheduling of membrane cleaning.

Author Contributions: Project conceptualization, supervision, resources, writing, funding acquisition, and project administration, and manuscript editing were carried out by Y.C., P.D.C., and L.G. Y.A.J. contributed to the manuscript writing, review, and editing, in addition to formal data analysis and validation. L.G. did the experimental work and initial preparation of the manuscript. All authors have read and agreed to the published version of the manuscript.

Funding: This work was supported, in part, by the UC/Office of the President (Award RP20407-004) and the California Department of Water Resources (DWR) in coordination with the National Alliance for Water Innovation/DOE, California Department of Water Resources (DWR) Agreement 4600014087(Award RP20407-004); California Water Resources Control Board (SWRCB000000000D14251550, C/A 367); California DWR Agreement 4600011630; US Department of the Interior, Bureau of Reclamation, Desalination and Water Purification Research (Grant R11AC81533); and the UCLA Water Technology Research (WaTeR) Center.

Data Availability Statement: The data is presented in the manuscript.

Acknowledgments: The authors acknowledge the contributions of Aihua Zhu and Alex Bartman for the formulation of the theoretical background, and the contributions of Anditya Rahardianto and John Thompson in various to various stages of the pilot plant construction and operation. The authors also acknowledge contributions of various pumps and related materials by Danfoss Sea Recovery (Henrik Wendelboe and Christopher Okada), UF membranes by Inge GmbH (Peter Berg, Martin Heijnen, and Josef Wunram), sensors and actuators by George Fisher (Rick Hines), and membrane elements by Toray Membranes USA. The Panoche Drainage District provided field site access and needed local infrastructure.

Conflicts of Interest: The authors declare no conflicts of interest.

Water 2025, 17, 2363 20 of 26

Appendix A

Appendix A.1. Pump Efficiencies

The efficiencies [36,45] of the RO first-stage feed and second-stage interstage pumps (Section 3.1) were determined experimentally (via monitoring of the pump power consumption at different flow rates and pressure head). The pump efficiencies were correlated with the flow rate (m³/h) and output pressure (bar) as per the following empirical equations:

$$\eta_1 = a_1 + a_2 \cdot exp \left[-0.5 \cdot \left(\frac{Q_f - a_3}{a_4} \right)^2 - 0.5 \cdot \left(\frac{\Delta P_1 - a_5}{a_6} \right)^2 \right]$$
 (A1a)

$$\eta_2 = b_1 + b_2 \cdot Q_{f2} + b_3 \cdot \Delta P_2 + b_4 \cdot Q_{f2}^2 + b_5 \cdot \Delta P_2^2$$
 (A1b)

in which the empirical constants for the RO first-stage feed pump (a_1 , a_2 , a_3 , a_4 , a_5 , a_6) and the second pump (b_1 , b_2 , b_3 , b_4 , b_5) are provided in Table A1, and where the empirical Equation (A1a) and Equation (A1b) prediction performances were with R² values of 0.98 and 0.96, respectively.

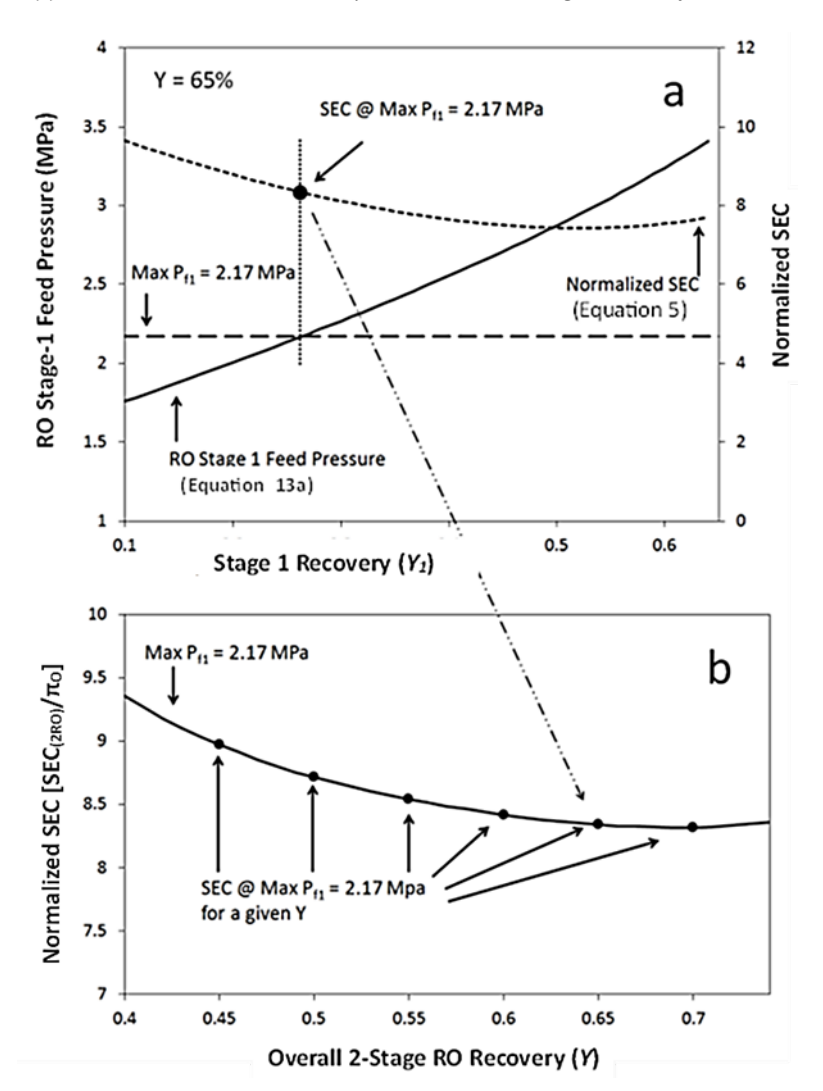
Table A1. Empirical constants for Pump Efficiency Correlations for the pumps of the first and second stages.

First Stage Pump Efficiency Parameters	Second Stage Pump Efficiency Parameters
(Equation (A1a))	(Equation (A1b))
$a_1 = 0.356$	$b_1 = 0.243$
$a_2 = 0.165$	$b_2 = 1.74 \times 10^{-3} \mathrm{m}^{-3} \mathrm{h}$
$a_3 = 29.516 \text{ m}^3/\text{h}$	$b_3 = 3.43 \times 10^{-4} \text{bar}^{-1}$
$a_4 = 12.487 \text{ m}^3/\text{h}$	$b_4 = 2.91 \times 10^{-4} \mathrm{m}^{-6} \mathrm{h}^2$
$a_5 = 435.758$ bar	$b_5 = -4.16 \times 10^{-7} \mathrm{bar}^{-1}$
a ₆ = 378.326 bar	

Appendix A.2. Concentration Polarization Modulus for Spiral-Wound RO Elements

The degree of concentration polarization for the RO elements was determined as per, whereby the concentration polarization modulus $\overline{CP} = Q_p / A_m k_f$, in which k_f is the feed-side mass transfer coefficient estimated from a Sherwood number correlation provided by the RO elements manufacturer, namely $Sh = k_f \cdot D / d_h = 0.38 Re^{0.54} Sc^{0.33}$ [52,53] in which the Reynolds (Re) and Schmidt (Sc) numbers are defined as Re = $(v \cdot dh \cdot \rho)/\mu$ and $Sc = \mu/D$, respectively, where the average crossflow velocity is given as $v = (Q_f + Q_e)/2A_e$, Q_f , Q_e and Q_p are the feed, concentrate and permeate flow rates, dh and A_e are the RO channel hydraulic radius and cross-sectional area, respectively, D is the solute molecular mass diffusivity and μ and ρ are the fluid viscosity and mass density, respectively. The values of A_m , dh and A_e for the first-stage elements were 113.2 m², 0.001 m and 0.00345 m², respectively, and 47.5 m², 0.00109 m and 0.0032 m² for the second-stage elements.

Water 2025, 17, 2363 21 of 26



Appendix A.3. Determination of the SEC vs. 2-Stage Recovery at the Maximum Stage 1 Pressure

Figure A1. (a) Illustration of the procedure for plotting the SEC versus overall recovery for operation at a given maximum Stage 1 feed pressure (P_{f1}) for targets overall permeate flow rate (Q_P) of 45.4 L/min, feed salinity of 24,676 mg/L. In the first step the first-stage feed pressure, P_{f1} , is calculated as a function of Y_1 using Equation (13a). The first-stage recovery, Y_1 , that corresponds to the max P_{f1} constraint can thus be obtained as shown in (**a**) as the intersection between the solid and dashed lines. The SEC at the Y_1 value is then calculated via Equation (5) and this value represents the SEC at the max P_{f1} constraint for a given Y. The above process is repeated for different Y values to obtain the SEC (at the max P_{f1} constraint) as a function of the overall recovery (Y), and the resulting curve is shown in (**b**).

Appendix A.4. SEC Optimization for a Scenario of Changing Feed Salinity

In order to evaluate the controller's performance subject to changes in feedwater salinity, for operation at fixed target permeate production, a short disturbance of increased feedwater salinity was introduced. This was achieved by diverting the RO concentrate to a feed tank where it was mixed with the raw feedwater to increase the feed salinity to the first RO stage. The flow rate of recycled RO concentrate was set to 6.94 L/min until the salinity of the water in the feed tank reached 24,190 mg/L TDS. The concentrate recycle flow rate was then gradually reduced until it was turned off over a period of 270 s. This produced a raw feed stream with a salinity that decreased from 24,190 mg/L mg/L TDS to 17,833 mg/L TDS over the above period (Figure A2a).

Water 2025, 17, 2363 22 of 26

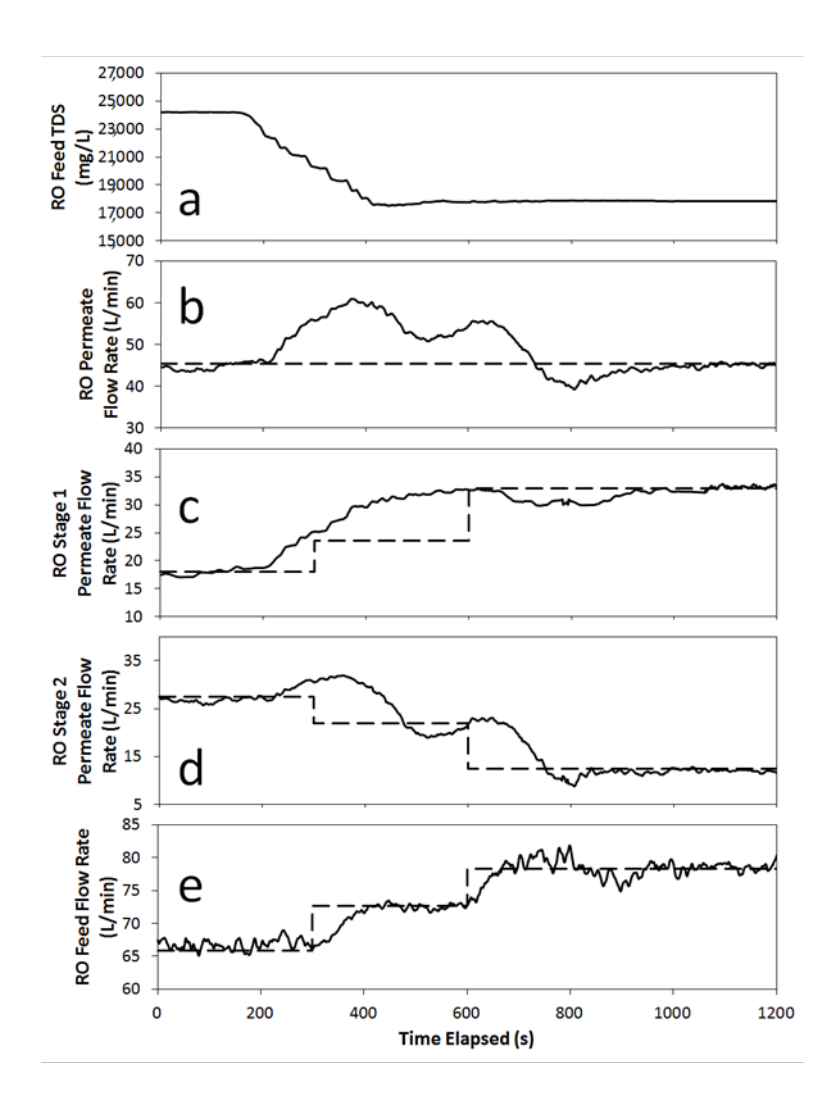


Figure A2. Profiles of (a) raw feedwater salinity, (b) RO permeate flow rate, (c) RO first-stage permeate flow rate, (d) RO second-stage permeate flow rate, and (e) RO feed flow rate with respect to time. The controller was iterated at 300 s and again at 600 s. Originally, the feed flow rate controller set-point was at 65.8 L/min 78.3 L/min. At 300 s, the controller went through an iteration while the feed salinity was changing, calculating a new set-point for feed flow rate of 72.6 L/min. At 600 s, the controller calculated the new 78.3 L/min feed flow rate set-point for the new high feed salinity.

In the above control test, the RO plant operated under energy-optimal RO control at an initial constant feed salinity of 24,190 mg/L with a permeate production set-point of 45.4 L/min, overall and first stage water recoveries of Y = 69% and $Y_1 = 27.3\%$, respectively (Figure A2). The optimal overall and first-stage recovery at which the system was initially operated was determined by the supervisory controller for the initial feed salinity of 24,190 mg/L (Figures A3 and A2). Here it is noted that the overall recovery for the RO plant was constraint in the range of 40%-74% and where the first-stage water recovery was constrained by the maximum Stage 1 pressure ($P_{f,1}$) limit of 2.17 MPa. The operation proceeded as guided by the energy-optimal controller, and at t = 160 s the feed salinity began its gradual decrease. At the approximate time of t = 300 s (140 s after commencing with the feed salinity decrease), the supervisory controller performed an iteration and determined a new energy-optimal operating state for the feed salinity measured at that moment (i.e., t = 300 s). At approximately t = 600 s (440 s after commencing with the prescribed feed salinity decrease and after the feed salinity reached the new steady-state value of 17,833 mg/L at about t = 400 s), the supervisory controller determined the energy-optimal operating state for the above feed salinity. For both iterations, the supervisory controller Water 2025, 17, 2363 23 of 26

established the maximum first-stage pressure (2.17 MPa) to be the energy-optimal operating set-point; thus, the first-stage pressure set-point did not change for either controller iteration. The only change in pressure was to decrease the second-stage pressure (Figure A4) from 3.63 MPa to 3.19 MPa, and then to 2.90 MPa. The final calculated operating condition for the feed salinity of 17,833 mg/L TDS was at Y = 58%, and $Y_1 = 41.5\%$. The transition between the two states is shown in Figures A2 and A4.

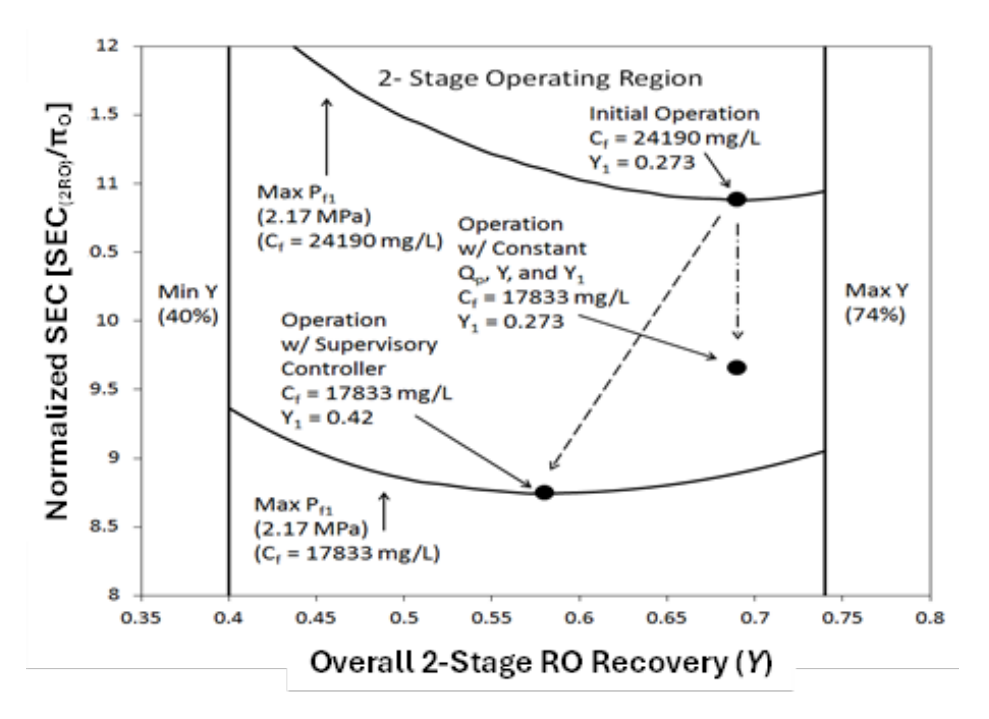


Figure A3. Normalized SEC with respect to overall system water recovery (Y), with the constraints of minimum Y (40%), maximum Y (74%), and maximum $P_{f,1}$ (2.17 MPa). Solid circles denote the controller established operating points. The arrows depict the transition between the initial and final operating states during feed salinity change under energy-optimal control (dashed line) operation for a constant permeate production (dash-dotted line). Note: the operational region bounded by the maximum Stage 1 feed pressure ($P_{f,1}$) was determined as illustrated in Appendix A.3.

The transition with respect to the SEC is shown in Figure A3 shows two unique SEC curves for the max P_{f^1} constraint at the initial and final feedwater salinity levels (Figure A3). Here it is noted that the Stage 1 pump efficiency is higher than that of the Stage 2 pump and increases further as Y_1 increases. When the feed salinity decreases for system operation at the max $P_{f,1}$, the Stage 1 permeate flow will increase and thus Y_1 will also increase. Therefore, the load on the less efficient Stage 2 pump will drive the optimal SEC, along the curve of SEC-Y curve at the max $P_{f,1}$ constraint, toward a lower optimal SEC (Figure A3). A comparison of the controller's SEC reduction relative to operation of the two-stage RO desalination plant in which the permeate flux in both stages is identical for a fixed target permeate production (i.e., flow rate) is also shown in Figure A3 for the above operational scenario, while the permeate water productivity is maintained the Stage 1 feed pressure is decreased to maintain a constant flux in this stage. Without an energy-optimal controller, the conventional approach of operating the two stages at the same permeate flux would lead SEC that is ~10% higher compared to operation with the energy-optimal controller.

Water 2025, 17, 2363 24 of 26

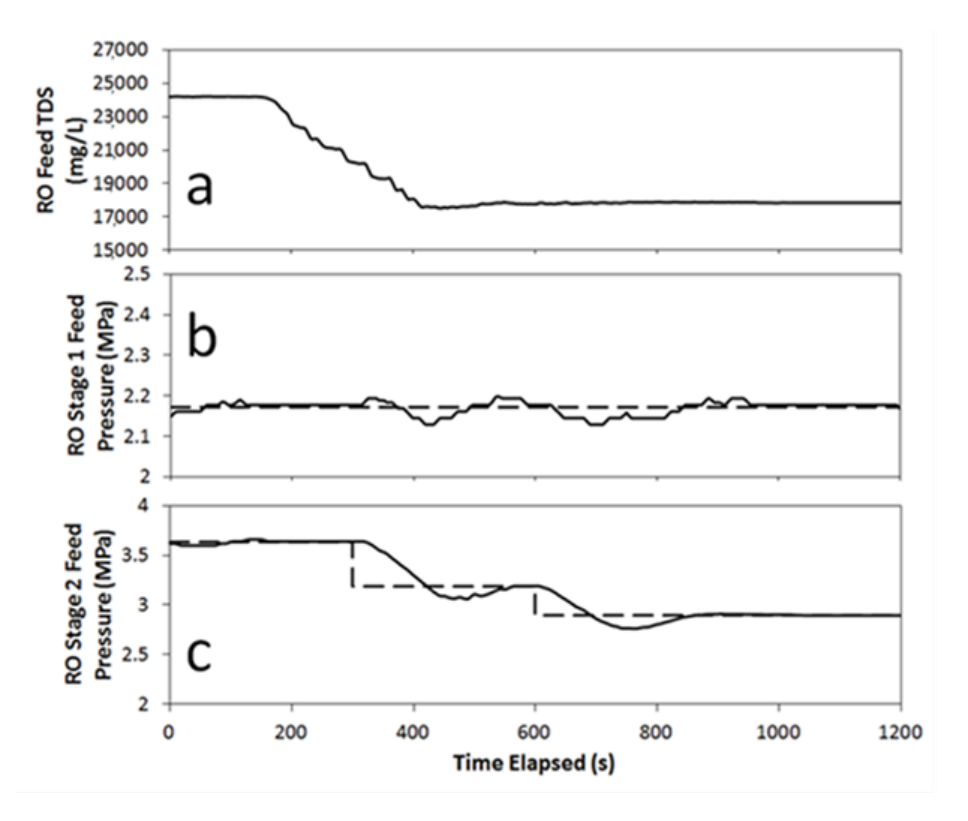


Figure A4. Profiles of (a) raw feedwater salinity, (b) RO Stage 1 feed pressure, and (c) RO Stage 2 feed pressure with respect to time. The controller iteration steps were at 300 s and again at 600 s. Initially, the lower-level controllers' feed pressure set-points were at 2.17 MPa, and 3.63 MPa for Stages 1 and 2, respectively. After the first iteration at 300 s, the Stage 2 feed pressure set-point changed to 3.34 MPa. The Stage 1 feed pressure set-point remained at 2.17 MPa since this was the maximum Stage 1 pressure constraint. After the second controller iteration at 600 s, the Stage 2 feed pressure set-point was set to 2.90 MPa.

References

- 1. Gray, S.; Semiat, R.; Duke, M.; Rahardianto, A.; Cohen, Y. Seawater Use and Desalination Technology. In *Treatise on Water Science*; Peter, W., Ed.; Elsevier: Oxford, UK, 2011; pp. 73–109.
- 2. Shemer, H.; Wald, S.; Semiat, R. Challenges and Solutions for Global Water Scarcity. Membranes 2023, 13, 612.
- 3. Alghoul, M.; Poovanaesvaran, P.; Sopian, K.; Sulaiman, M. Review of brackish water reverse osmosis (BWRO) system designs. *Renew. Sustain. Energy Rev.* **2009**, *13*, 2661–2667.
- 4. Committee on Advancing Desalination. *Technology. Desalination: A National Perspective*; National Academies Press: Washington, DC, USA, 2008.
- 5. Cohen, Y. Advances in Water Desalination Technologies; World Scientific Publishing Company: Singapore, 2021.
- 6. Harby, K.; Emad, M.; Benghanem, M.; Abolibda, T.Z.; Almohammadi, K.; Aljabri, A.; Alsaiari, A.; Elgendi, M. Reverse osmosis hybridization with other desalination techniques: An overview and opportunities. *Desalination* **2024**, *581*, 117600.
- 7. Mickley, M.C. Membrane Concentrate Disposal: Practices and Regulation; Desalination and Water Purification Research and Development Program Report 123 (Second Edition), Mickley and Associates, Agreement No. 98-FC-81-0054; US Department of the Interior, Bureau of Reclamation, Technical Service Center: Denver, CO, USA, April 2006. Available online: https://www.usbr.gov/research/dwpr/reportpdfs/report123.pdf (accessed on 3 August 2025).
- 8. Gabelich, C.J.; Xu, P.; Cohen, Y. Concentrate treatment for inland desalting. Sustain. Sci. Eng. 2010, 2, 295–326.
- 9. Drak, A.; Adato, M. Energy recovery consideration in brackish water desalination. Desalination 2014, 339, 34–39.
- 10. Kremen, S.; Wilf, M.; Lange, P. Operating results and economics of single stage and two stage large size sea water RO systems. *Desalination* **1991**, *82*, 3–13.
- 11. Cardona, E.; Piacentino, A.; Marchese, F. Energy saving in two-stage reverse osmosis systems coupled with ultrafiltration processes. *Desalination* **2005**, *184*, 125–137.

Water 2025, 17, 2363 25 of 26

12. Zhu, A.Z.; Christofides, P.D.; Cohen, Y. Effect of thermodynamic restriction on energy cost optimization of RO membrane water desalination. *Ind. Eng. Chem. Res.* **2009**, *48*, 6010–6021.

- 13. Wei, Q.J.; McGovern, R.K. Saving energy with an optimized two-stage reverse osmosis system. *Environ. Sci. Water Res. Technol.* **2017**, *3*, 659–670.
- 14. Al-Obaidi, M.; Kara-Zaïtri, C.; Mujtaba, I. Significant energy savings by optimising membrane design in the multi-stage reverse osmosis wastewater treatment process. *Environ. Sci. Water Res. Technol.* **2018**, *4*, 449–460.
- 15. Kabeel, A.; Abdelgaied, M. Optimized number of multi-stage spiral-wound reverse osmosis connected in series to achieves minimum power consumptions. *AIP Conf. Proc.* **2023**, *2801*, 030010.
- 16. Kim, J.; Park, K.; Hong, S. Optimization of two-stage seawater reverse osmosis membrane processes with practical design aspects for improving energy efficiency. *J. Membr. Sci.* **2020**, *601*, 117889.
- 17. Ghasemi, Z.; MirBagheri, S.; Vafaei, F. Optimization of a two-stage reverse osmosis pilot system for Caspian seawater desalination using response surface methodology: SEC reduction through recovery increase, Fe fouling, and scaling control. *Int. J. Environ. Sci. Technol.* **2024**, 21, 493–514.
- 18. Mehrizi, R.A.; Mirbagheri, S.A.; Shams, A. Development of a generalized mathematical model for two-stage reverse osmosis desalination systems. *Comput. Chem. Eng.* **2024**, *182*, 108562.
- 19. Lee, T.; Rahardianto, A.; Cohen, Y. Flexible reverse osmosis (FLERO) desalination. Desalination 2019, 452, 123–131.
- 20. Hosseinipour, E.; Harris, E.; El Nazer, H.A.; Mohamed, Y.M.; Davies, P.A. Desalination by batch reverse osmosis (RO) of brackish groundwater containing sparingly soluble salts. *Desalination* **2023**, *566*, 116875.
- 21. Warsinger, D.M.; Tow, E.W.; Nayar, K.G.; Maswadeh, L.A. Energy efficiency of batch and semi-batch (CCRO) reverse osmosis desalination. *Water Res.* **2016**, *106*, 272–282.
- 22. Kim, J.; Dong, L.; Shon, H.K.; Park, K. Current progress in semi-batch reverse osmosis for brackish water desalination. *Desalination* **2024**, *578*, 117434.
- 23. Kim, M.; Jeon, J.; Ryu, H.; Lee, S.; Kim, S. Assessment of energy saving effects in membrane-based seawater desalination. *Desalination Water Treat.* **2017**, 77, 149–155.
- 24. Al-Obaidi, M.A.; Rasn, K.H.; Aladwani, S.; Kadhom, M.; Mujtaba, I. Flexible design and operation of multi-stage reverse osmosis desalination process for producing different grades of water with maintenance and cleaning opportunity. *Chem. Eng. Res. Des.* 2022, 182, 525–543.
- 25. Kim, Y.; Park, Y.-G.; Park, K. Optimal design strategy, heuristics, and theoretical analysis of multi-stage reverse osmosis for seawater desalination. *Desalination* **2024**, *580*, 117534.
- 26. Nour-Mohammad, M.; Fakhroleslam, M. Sustainable Reverse Osmosis Desalination Systems: Comprehensive Superstructure Modeling and Multi-Objective Optimization. *Ind. Eng. Chem. Res.* **2025**, *64*, 6580–6595.
- 27. Abkar, L.; Mehrizi, A.A.; Jafari, M.; Beck, S.E.; Ghassemi, A.; Van Loosdrecht, M.C. Optimizing energy efficiency in brackish water reverse osmosis (BWRO): A comprehensive study on prioritizing critical operating parameters for specific energy consumption minimization. *Sci. Total Environ.* **2024**, 932, 172772.
- 28. Taniguchi, M.; Kurihara, M.; Kimura, S. Behavior of a reverse osmosis plant adopting a brine conversion two-stage process and its computer simulation. *J. Membr. Sci.* **2001**, *183*, 249–257.
- 29. Lu, Y.Y.; Hu, Y.D.; Zhang, X.L.; Wu, L.Y.; Liu, Q.Z. Optimum design of reverse osmosis system under different feed concentration and product specification. *J. Membr. Sci.* 2007, 287, 219–229.
- 30. Manth, T.; Gabor, M.; Oklejas, E. Minimizing RO energy consumption under variable conditions of operation. *Desalination* **2003**, 157, 9–21.
- 31. Sprintall, J.; Potemra, J.T.; Hautala, S.L.; Bray, N.A.; Pandoe, W.W. Temperature and salinity variability in the exit passages of the Indonesian Throughflow. *Deep. Sea Res. Part II Top. Stud. Oceanogr.* **2003**, *50*, 2183–2204.
- 32. Pace, N.G.; Jensen, F.B. *Impact of Littoral Environmental Variability on Acoustic Predictions and Sonar Performance*; Springer Science and Business Media: Dordrecht, The Netherlands, 2002.
- 33. Morey, S.L.; Dukhovskoy, D.S. Analysis Methods for Characterizing Salinity Variability from Multivariate Time Series Applied to the Apalachicola Bay Estuary. *J. Atmos. Ocean. Technol.* **2012**, *29*, 613–628.
- 34. Kurihara, M. Sustainable seawater reverse osmosis desalination as green desalination in the 21st century. *J. Membr. Sci. Res.* **2020**, *6*, 20–29.
- 35. Gao, L.; Rahardianto, A.; Gu, H.; Christofides, P.D.; Cohen, Y. Energy-optimal control of RO desalination. *Ind. Eng. Chem. Res.* **2014**, 53, 7409–7420.
- 36. Li, M. Optimal plant operation of brackish water reverse osmosis (BWRO) desalination. Desalination 2012, 293, 61-68.

Water 2025, 17, 2363 26 of 26

37. Lee, S.; Hong, J.; Har, D. Jointly optimized control for reverse osmosis desalination process with different types of energy resource. *Energy* **2016**, *117*, 116–130.

- 38. Yun, B.; Cho, K.H.; Shim, J. Towards autonomous operation of two-stage reverse osmosis water treatment system with multiagent reinforcement learning. *Desalination* **2025**, *609*, 118870.
- 39. Gordon, J.M.; Hui, T.C. Thermodynamic perspective for the specific energy consumption of seawater desalination. *Desalination* **2016**, *386*, 13–18.
- 40. Mulder, M. Basic Principles of Membrane Technology; Kluwer Academic Publishers: Boston, MA, USA, 1997.
- 41. DuPont. FilmTecTM Reverse Osmosis Membranes, Technical Manual, Version 17, 2024. Available online: https://www.dupont.com/content/dam/water/amer/us/en/water/public/documents/en/RO-NF-FilmTec-Manual-45-D01504-en.pdf (accessed on 3 August 2025).
- 42. *ASTM D4516*; Standard Practice for Standardizing Reverse Osmosis Performance Data. ASTM International: West Conshohocken, PA, USA, 2010.
- 43. Hydranautics. Foulants and Cleaning Procedures for Composite Polyamide RO/NF Membrane Elements; Hydranautics: Oceanside, CA, USA, 2020.
- 44. Karassik, I.J.; Messina J.P.; Cooper, P.; Heald, C.C. *Pump Handbook*, 3rd ed.; McGraw-Hill: London, UK, 2001. Available online: https://www.google.com/books/edition/Pump_Handbook_Third_Edition/wOvCwgEACAAJ?hl=en (accessed on 3 August 2025).
- 45. Li, M.; Noh, B. Validation of model-based optimization of brackish water reverse osmosis (BWRO) plant operation. *Desalination* **2012**, *304*, 20–24.
- 46. Boggs, P.T.; Tolle, J.W. Sequential Quadratic Programming. Acta Numer. 1995, 4, 1–51.
- 47. Anbu, S.; Senthilkumar, M.; Murugesh, T.S. Design of a Multiloop Controller for a Nonlinear Process. *Int. J. Adv. Comput. Sci. Appl.* **2022**, *13*, 290–299.
- 48. Vu, T.N.L.; Lee, M. Independent design of multi-loop PI/PID controllers for interacting multivariable processes. *J. Process Control* **2010**, *20*, 922–933.
- 49. Ellis, M.; Durand, H.; Christofides, P.D. A Tutorial Review of Economic Model Predictive Control Methods. *J. Process Control* **2014**, 24, 1156–1178.
- 50. Wang, Z.; We, P. Analytical Multiloop Control for Multivariable Systems with Time Delays. *Complexity* **2020**, *9*, 8849483. https://doi.org/10.1155/2020/8849483.
- 51. Seborg, D.E.; Edgar, T.F.; Mellichamp, D.A. *Process Dynamics and Control*, 2nd ed.; John Wiley and Sons, Inc.: Danvers, MA, USA, 2004.
- 52. Oh, H.J.; Hwang, T.M.; Lee, S. A simplified simulation model of RO systems for seawater desalination. *Desalination* **2009**, 238, 128–139.
- 53. Sablani, S.; Goosen, M.; Al-Belushi, R.; Wilf, M. Concentration polarization in ultrafiltration and reverse osmosis: A critical review. *Desalination* **2001**, 141, 269–289.

Disclaimer/Publisher's Note: The statements, opinions and data contained in all publications are solely those of the individual author(s) and contributor(s) and not of MDPI and/or the editor(s). MDPI and/or the editor(s) disclaim responsibility for any injury to people or property resulting from any ideas, methods, instructions or products referred to in the content.